INTERNATIONAL JOURNAL FOR NUMERICAL METHODS IN ENGINEERING
Int. J. Numer. Meth. Engng. 2000; **47**:1569–1603

Accurate radiation boundary conditions for the time-dependent wave equation on unbounded domains

Runnong Huan and Lonny L. Thompson*,†

Department of Mechanical Engineering, Clemson University, Clemson, SC 29634, U.S.A.

SUMMARY

Asymptotic and exact local radiation boundary conditions (RBC) for the scalar time-dependent wave equation, first derived by Hagstrom and Hariharan, are reformulated as an auxiliary Cauchy problem for each radial harmonic on a spherical boundary. The reformulation is based on the hierarchy of local boundary operators used by Bayliss and Turkel which satisfy truncations of an asymptotic expansion for each radial harmonic. The residuals of the local operators are determined from the solution of parallel systems of linear first-order temporal equations. A decomposition into orthogonal transverse modes on the spherical boundary is used so that the residual functions may be computed efficiently and concurrently without altering the local character of the finite element equations. Since the auxiliary functions are based on residuals of an asymptotic expansion, the proposed method has the ability to vary separately the radial and transverse modal orders of the RBC. With the number of equations in the auxiliary Cauchy problem equal to the transverse mode number, this reformulation is exact. In this form, the equivalence with the closely related non-reflecting boundary condition of Grote and Keller is shown. If fewer equations are used, then the boundary conditions form high-order accurate asymptotic approximations to the exact condition, with corresponding reduction in work and memory. Numerical studies are performed to assess the accuracy and convergence properties of the exact and asymptotic versions of the RBC. The results demonstrate that the asymptotic formulation has dramatically improved accuracy for time domain simulations compared to standard boundary treatments and improved efficiency over the exact condition. Copyright © 2000 John Wiley & Sons, Ltd.

KEY WORDS: radiation boundary conditions; non-reflecting boundary conditions; wave equation; finite element method; scattering; unbounded domains

1. INTRODUCTION

Direct time-domain solutions of the scalar wave equation on unbounded domains follows from the need to accurately simulate radiation and scattering from pulse-driven structures of arbitrary

*Correspondence to: Lonny L. Thompson, Department of Mechanical Engineering, Clemson University, 102 Fluor Daniel Engineering Innovation Building, PO Box 340921, Clemson, SC 29634-0921, U.S.A.
†E-mail: lonny.thompson@ces.clemson.edu

Contract/grant sponsor: National Science Foundation; contract/grant number: CMS-9702082
Contract/grant sponsor: PECASE

CCC 0029-5981/2000/091569–35$17.50

Received 12 March 1999
Revised 7 July 1999

shape. In theory, the exact time-dependent solution may be determined from the retarded potential formulation of the well-known Kirchoff integral representation [1, 2] applied on the surface of the scatterer. However, because the surface integrals must be discretized in both temporal and spatial domains simultaneously, the time convolution of all surface points must be stored, resulting in large memory and work requirements. In addition, numerical instabilities may result [3]. A stabilized version has recently been developed in Reference [4], although the problem of the storage of time histories remains.

Another direct approach is to exploit the finite wave speed c, in the unbounded medium, and extend the computational domain using explicit solvers on an 'infinite grid' so that the boundary cannot influence the solution in the region of interest for times less than the final time T. Solutions obtained in this way would require field calculations in the region between the source and the distant points of interest. This would require a large mesh/grid of width of order $O(cT)$, with corresponding increase in computer expense and memory. Even with the use of explicit time integrators, direct field calculations for points distant from a radiating structure or scatterer are generally impractical for moderate to large times.

For this reason, when solving unbounded problems with a domain-based computational method such as the finite element method, the far-field is truncated at an artificial boundary surrounding the source of radiation or a scatterer. The impedance of the far-field is then represented on this boundary by either approximate radiation boundary conditions, infinite elements, or absorbing sponge layers. Survey articles of various boundary treatments are given in References [5, 6]. Efficient evaluation of accurate boundary treatments for the time-dependent wave equation on unbounded spatial domains has long been an obstacle for the development of reliable solvers for time domain simulations. Ideally, the artificial boundary would be placed as close as possible to the scatterer, and the radiation boundary treatment would be capable of arbitrary accuracy at a cost and memory not exceeding that of the interior solver.

If the form of the boundary treatment is oversimplified, spurious reflected waves can be generated at the artificial boundary, which can substantially degrade the accuracy of the numerical solution. For example, a standard approach is to apply the local (differential) boundary operators derived by Bayliss and Turkel [7] which annihilate leading terms in a radial asymptotic expansion for outgoing wave solutions. However, as the order of these local non-reflecting boundary conditions increases they become increasingly difficult to implement in standard numerical methods due to the occurrence of high-order derivatives on the artificial boundary.

To overcome this difficulty, Ting and Miksis [8, 9] formulated an exact non-reflecting boundary condition which makes use of the Kirchoff integral formula on the artificial boundary Γ and a convolution requiring storage of the solution time-history at a surface inside Γ for the time needed for waves to propagate across the computational domain. While, this approach improves both cost and storage compared to direct implementation of the retarded potential form of the Kirchoff integral, it does not appear to be competitive on cost compared to equally accurate treatments discussed below.

In recent years, a number of new boundary treatments have been developed which have dramatically improved both the accuracy and efficiency of time domain simulations. These new developments include fast spherical harmonic evaluation of exact, local in time boundary conditions on spherical boundaries [10–15], rational approximations to the DtN kernel [16], absorbing sponge layers with reflectionless interfaces [17, 18], and recursive methods of implementing high-order sequences of space and time localized radiation boundary conditions [19].

For time-harmonic problems, exact non-reflecting boundary conditions applied to a separable boundary are available through Fourier or Laplace transform methods and the so-called

Dirichlet-to-Neumann (DtN) map [20–25]. The DtN map is a non-local (integral) operator obtained from the trace of the normal derivative of the solution on the truncation boundary. For the sphere, the DtN kernel involves spherical Hankel functions, which may be represented in terms of simple rational functions. The rationality of the DtN kernel implies that the temporal convolution of the time-dependent counterpart can be localized, making computation efficient. The time localization of the exact DtN boundary condition was first recognized and used in References [10, 11, 26–28]. In Reference [26], the time-convolution integral is approximated using special recurrence formulae. In References [27, 28], the convolution is replaced with high-order time derivatives which may be implemented in discontinuous Galerkin space–time finite element methods. In Reference [10], a local in time representation is obtained by solution of an auxiliary Cauchy problem for linear first-order systems of ordinary differential equations on the boundary for each spherical harmonic. The implementation of this local-in-time representation of the DtN map using finite difference methods is discussed in Reference [11]. In Reference [12] we showed how to implement the NRBC in a standard semidiscrete finite element formulation with several alternative implicit and explicit time integrators. In Reference [12], the NRBC is rederived based on direct application of a result given in Lamb [29], with improved scaling of the first-order system of equations associated with the NRBC.

In Reference [13], a modified version of the exact NRBC first derived in Reference [11], is implemented in a finite element formulation using a standard implicit time-integrator for the semidiscrete equations concurrently with the Cauchy problem for each mode. In order to obtain a symmetric system, the NRBC is reformulated with additional auxiliary variables on the truncation boundary. The modified version may be viewed as an extension of the second-order local boundary operator derived by Bayliss and Turkel [7], and gives improved accuracy when only a few harmonics are included in the spherical expansion/transformation. Extensions to the semi-infinite problem resulting from transducers or vibrating structures mounted in a half-plane are given in Reference [14]. In Reference [14] we also show how standard explicit time integrators may be used to solve the semidiscrete finite element equations concurrently with implicit solvers for the auxiliary variables in the modified boundary condition formulated in Reference [13]. In Reference [15], a method is described for calculating far field solutions concurrently with the near-field solution based on the exact NRBC. At each discrete time step, radial modes computed on a spherical artificial boundary which drive the exact NRBC for the near-field solution, are imposed concurrently as data for the radial wave equation in the far-field. The radial grid is truncated at the far-field point of interest with the modal form of the exact NRBC. The solution in the far-field is then computed from an inverse spherical harmonic transform of the radial modes.

Hagstrom and Hariharan [19] have derived a sequence of radiation boundary conditions involving first-order differential equations in time and tangential derivatives of auxiliary functions on a circular or spherical boundary. They indicate how these local conditions may be effectively implemented in a finite difference scheme using only local tangential operators, but at the cost of introducing a large number of auxiliary functions at the boundary. Numerical experiments were conducted for a model problem involving the Fourier modes of the wave equation in two dimensions using a finite difference method. However, consistent finite element implementation of this sequence in a standard Galerkin variational equation would result in a non-symmetric coupled system of equations.

In this paper we rederive the sequence of local boundary conditions described in Reference [19] based on the hierarchy of local boundary operators used by Bayliss and Turkel and a recursion relation for the expansion coefficients appearing in a radial asymptotic (multipole) expansion. We then

reformulate in terms of spherical harmonics by using a decomposition into orthogonal transverse modes. The resulting procedure then involves a Cauchy problem involving systems of first-order temporal equations, similar to that used in References [10, 12]. A modified version similar to the formulation given in Reference [13] is also reported. With this reformulation, the auxiliary functions are recognized as residuals of the local boundary operators acting on the asymptotic expansion, and may be implemented efficiently and in parallel with standard semidiscrete finite element methods without changing the symmetric and banded/sparse structure of the matrix equations. Since the auxiliary functions are based on residuals of decreasing order, the proposed method has the ability to vary separately the radial and transverse modal orders of the radiation boundary condition. With the number of time-dependent auxiliary variables in the Cauchy problem for each radial mode equal to the transverse mode number, this reformulation is exact. If fewer equations are used, then the boundary conditions form high-order accurate asymptotic approximations to the exact condition, with corresponding reduction in work and memory. For the exact version, we establish the equivalence to the exact non-reflecting boundary conditions derived in References [10, 12] and identify several distinct advantages of the asymptotic form of the radiation boundary condition compared to the NRBC given in References [10, 12].

Both total field and scattered field finite element formulations are presented for implementing the radiation boundary conditions. When directly solving the total field, the variational equation is modified to represent the incident wave field on the radiation boundary. Numerical studies are performed and compared to analytical solutions to assess the accuracy and convergence properties of the radiation boundary conditions. Numerical examples include steady multipole radiation of individual harmonics, radiation/scattering problems involving an infinite number of modes, and transient radiation from a circular transducer mounted in an infinite planar baffle.

2. INITIAL-BOUNDARY VALUE PROBLEM

We consider time-dependent scattering and radiation of waves in an infinite three-dimensional region $\mathscr{R} \subset \mathbb{R}^3$, surrounding an object with surface $\mathscr{S}$. For computation, the unbounded region $\mathscr{R}$ is truncated by an artificial spherical boundary Γ, of radius $\|\mathbf{x}\| = R$. We then denote by $\Omega \subset \mathscr{R}$, the finite subdomain bounded by $\partial\Omega = \Gamma \cup \mathscr{S}$, see Figure 1. Within Ω, the solution $\phi(\mathbf{x}, t) : \Omega \times [0, T] \mapsto \mathbb{R}$, satisfies the scalar wave equation

$$\frac{1}{c^2}\frac{\partial^2 \phi}{\partial t^2} = \nabla^2 \phi + f(\mathbf{x}, t), \quad \mathbf{x} \in \Omega, \ t \in [0, T] \tag{1}$$

with initial conditions

$$\phi(\mathbf{x}, 0) = \phi_0(\mathbf{x}), \quad \dot{\phi}(\mathbf{x}, 0) = \dot{\phi}_0(\mathbf{x}), \quad \mathbf{x} \in \Omega \tag{2}$$

and driven by the time-dependent radiation boundary condition on the surface $\mathscr{S}$:

$$\alpha\frac{\partial \phi}{\partial n} + \beta\frac{\partial \phi}{\partial t} + \gamma\phi = g(\mathbf{x}, t), \quad \mathbf{x} \in \mathscr{S}, \quad t \in [0, T] \tag{3}$$

In linear acoustics, the scalar function ϕ may represent the pressure field or a velocity potential. The wave speed c, and α, β, γ are real, and we assume $c > 0$, and $\alpha, \beta \geqslant 0$. The source f and initial data ϕ_0 and $\dot{\phi}_0$ are assumed to be confined to the computational domain Ω, so that in the

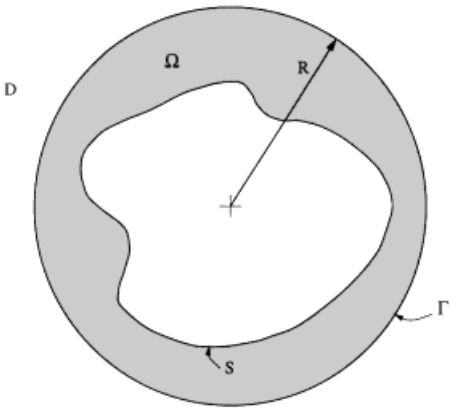

Figure 1. Illustration of unbounded region $\mathscr{R}$ surrounding a scatterer $\mathscr{S}$. The computational domain $\Omega \subset \mathscr{R}$ is surrounded by a spherical truncation boundary Γ of radius R, with exterior region $\mathscr{D} = \mathscr{R} - \Omega$.

exterior region $\mathscr{D} = \mathscr{R} - \Omega$, i.e. the infinite region outside Γ, the scalar field $\phi(\mathbf{x}, t)$ satisfies the homogeneous form of the wave equation

$$\frac{1}{c^2}\frac{\partial^2 \phi}{\partial t^2} = \nabla^2 \phi, \quad \mathbf{x} \in \mathscr{D}, \quad t \in [0, T] \tag{4}$$

$$\phi(\mathbf{x}, 0) = 0, \quad \dot{\phi}(\mathbf{x}, 0) = 0, \quad \mathbf{x} \in \Omega \tag{5}$$

In spherical co-ordinates (r, θ, φ), the external region is defined as

$$\mathscr{D} = \{r \geqslant R,\ 0 \leqslant \theta \leqslant \pi,\ 0 \leqslant \varphi < 2\pi\} \tag{6}$$

and the wave equation takes the form

$$\frac{1}{c^2}\frac{\partial^2 \phi}{\partial t^2} = \frac{\partial^2 \phi}{\partial r^2} + \frac{2}{r}\frac{\partial \phi}{\partial r} + \frac{1}{r^2}\Delta_\Gamma \phi \tag{7}$$

where

$$\Delta_\Gamma \phi = \frac{1}{\sin\,\theta}\frac{\partial}{\partial \theta}\left(\sin\,\theta \frac{\partial \phi}{\partial \theta}\right) + \frac{1}{\sin^2 \theta}\frac{\partial^2 \phi}{\partial \varphi^2} \tag{8}$$

is the spherical Laplacian. The general solution to (7) is given by the spherical harmonic expansion

$$\phi(r, \theta, \varphi, t) = \sum_{n=0}^{\infty} \sum_{m=-n}^{n} \phi_{nm}(r, t)\ Y_{nm}(\theta, \varphi) \tag{9}$$

where Y_{nm} are orthogonal spherical harmonics normalized on a unit sphere:

$$Y_{nm}(\theta, \varphi) = \frac{1}{\sqrt{N_{nm}}} P_n^{|m|}(\cos\,\theta)\, \mathrm{e}^{\mathrm{i}m\varphi} \tag{10}$$

defined by associated Legendre functions P_n^m, sine and cosine functions, and normalization factor

$$N_{nm} = \frac{4\pi(n + |m|)!}{(2n + 1)(n - |m|)!} \tag{11}$$

The spherical harmonics are eigenfunctions of the spherical Laplacian:

$$\Delta_\Gamma Y_{nm} = -n(n+1)Y_{nm} \tag{12}$$

The time-dependent modes $\phi_{nm}(r,t)$ satisfy the radial wave equation

$$\frac{1}{c^2}\frac{\partial^2 \phi_{nm}}{\partial t^2} = \left[\frac{\partial^2}{\partial r^2} + \frac{2}{r}\frac{\partial}{\partial r} - \frac{n(n+1)}{r^2}\right]\phi_{nm}, \quad r \geqslant R, \quad t \geqslant 0 \tag{13}$$

$$\phi_{nm}(r,0) = 0, \quad \dot{\phi}_{nm}(r,0) = 0, \quad r \geqslant R \tag{14}$$

For outgoing waves, the solution to (13) may be represented by the radial asymptotic (multipole) expansion:

$$\phi_{nm}(r,t) = \sum_{k=0}^{n} r^{-k-1}\phi_{nm}^k(r-ct) \tag{15}$$

Substituting (15) into (13), we obtain the recursion relation for derivatives of the wave functions appearing in the radial harmonic expansion:

$$(\phi_{nm}^k)' = c_n^k \ \phi_{nm}^{k-1}, \quad k = 1,2,\ldots,n \tag{16}$$

where

$$c_n^k = \frac{k(k-1) - n(n+1)}{2k} \tag{17}$$

3. CONSTRUCTION OF RADIATION BOUNDARY CONDITIONS

In the following, we rederive the high-order accurate radiation boundary conditions of Hagstrom and Hariharan [19], and then reformulate in terms of spherical harmonics. Here we use the hierarchy of local operators of Bayliss and Turkel [7] which annihilate radial terms in the asymptotic expansion (15). On a sphere, the local operators are easily constructed using a product of radial derivatives:

$$B_p = L_p(L_{p-1}(\cdots(L_2(L_1)))) \tag{18}$$

$$L_j = \left(\frac{1}{c}\frac{\partial}{\partial t} + \frac{\partial}{\partial r} + \frac{2j-1}{r}\right) \tag{19}$$

However, the product form $B_p\phi_{nm}$, involves high-order radial derivatives which limits the order p, which can be practically used in a numerical method. Inspired by the local boundary conditions of Hagstrom and Hariharan [19], involving a sequence of first-order equations in time with tangential derivatives, we reformulate the Bayliss and Turkel boundary operators as a recursive sequence involving first-order time derivatives only for each mode. This sequence is then cast as a system of first-order differential equations in time, for each harmonic, which may be solved concurrently with the finite element equations.

We interpret the residuals of the Bayliss and Turkel operators (18) acting on the asymptotic expansion (15) as a sequence of functions with reduced radial order. We apply $B_1 = L_1$ to the

radial expansion (15), with the result

$$B_1\,\phi_{nm} = \left(\frac{1}{c}\frac{\partial}{\partial t} + \frac{\partial}{\partial r} + \frac{1}{r}\right)\phi_{nm} = w^1_{nm} \tag{20}$$

$$w^1_{nm}(r,t) = \sum_{k=1}^{n} -k\,r^{-k-2}\phi^k_{nm} \tag{21}$$

The function w^1_{nm} defines the remainder of the radial expansion.

As noted by Bayliss and Turkel, $w^1_{nm}(r,t) = O(r^{-2})\phi_{nm} = O(r^{-3})$. If we set $w^1_{nm} = 0$, then $B_1\phi_{nm} = 0$. Applying the spherical harmonic expansion to this result; i.e. multiplying by Y_{nm}, summing over indices n and m, and evaluating on the artificial boundary at $r = R$, gives

$$B_1\,\phi = 0 \quad \text{on } \Gamma \tag{22}$$

which defines the first-order local boundary condition of Bayliss and Turkel. This approximate boundary condition is exact for waves propagating with the first harmonic corresponding to $n = 0$, however, for harmonics $n \geqslant 1$, the error is $O(R^{-3})$.

Next, we apply $B_2 = L_2(L_1)$ to (15)

$$B_2\,\phi_{nm} = \left(\frac{1}{c}\frac{\partial}{\partial t} + \frac{\partial}{\partial r} + \frac{3}{r}\right)(B_1\phi_{nm}) = L_2(w^1_{nm}) = w^2_{nm} \tag{23}$$

with remainder

$$w^2_{nm}(r,t) = \sum_{k=2}^{n} k(k-1)r^{-k-3}\phi^k_{nm} \tag{24}$$

We note that the residual of the second-order operator has the property $w^2_{nm}(r,t) = O(r^{-4})\phi_{nm} = O(r^{-5})$. Comparing to w^1_{nm}, the order is reduced. Setting $w^2_{nm} = 0$, multiplying by Y_{nm}, summing over n and m, and evaluating at $r = R$, defines the second-order local boundary condition of Bayliss and Turkel

$$B_2\,\phi = 0 \quad \text{on } \Gamma \tag{25}$$

This condition is exact for the harmonics $n = 0, 1$, with error $O(R^{-5})$ for $n \geqslant 2$.

In general, applying B_{j+1} to (15), we have by induction

$$B_{j+1}\,\phi_{nm} = \left(\frac{1}{c}\frac{\partial}{\partial t} + \frac{\partial}{\partial r} + \frac{2j+1}{r}\right)(B_j\phi_{nm}) = L_{j+1}(w^j_{nm}) = w^{j+1}_{nm} \tag{26}$$

where the residual of B_j is defined as

$$w^j_{nm}(r,t) = \sum_{k=j}^{n} a^j_k\,r^{-k-j-1}\phi^k_{nm} \tag{27}$$

$$a^j_k = (-1)^j k(k-1)\cdots(k-(j-1)) = (-1)^j\frac{k!}{(k-j)!} \tag{28}$$

We note the order of the residuals are reduced, $w^{j+1}_{nm} = O(r^{-2})w^j_{nm}$, $w^j_{nm}(r,t) = O(r^{-2j})\phi_{nm} = O(r^{-2j-1})$, and $B_j\phi_{nm} = 0$ is exact for harmonics $n < j$. For $j = 0$, we rewrite (20) as

$$L_1\,(w^0_{nm}) = \left(\frac{1}{c}\frac{\partial}{\partial t} + \frac{\partial}{\partial r} + \frac{1}{r}\right)w^0_{nm} = w^1_{nm} \tag{29}$$

where

$$w_{nm}^0(r,t) = \sum_{k=0}^{n} a_k^0 \, r^{-k-1} \phi_{nm}^k = \phi_{nm}(r,t) \tag{30}$$

For $j = 1, 2, \ldots, p_n$ we eliminate radial derivatives in Equation (26) in favour of a recursive sequence for w_{nm}^j. To this end we rewrite

$$L_{j+1}(w_{nm}^j) = \left(\frac{1}{c} \frac{\partial}{\partial t} + \frac{\partial}{\partial r} + \frac{2j+1}{r} \right) w_{nm}^j = w_{nm}^{j+1} \tag{31}$$

as

$$\frac{1}{c} \frac{\partial w_{nm}^j}{\partial t} = \frac{1}{2} w_{nm}^{j+1} - \frac{j}{r} w_{nm}^j - \frac{1}{2} \left(\frac{\partial}{\partial r} + \frac{1}{r} - \frac{1}{c} \frac{\partial}{\partial t} \right) w_{nm}^j \tag{32}$$

Now consider the last term in the brackets

$$\left(\frac{\partial}{\partial r} + \frac{1}{r} - \frac{1}{c} \frac{\partial}{\partial t} \right) w_{nm}^j = \sum_{k=j}^{n} a_k^j r^{-k-j-1} \{ 2(\phi_{nm}^k)' - (k+j) r^{-1} \phi_{nm}^k \} \tag{33}$$

Substituting the recursion relation for $(\phi_{nm}^k)'$ given in (16), and the definition for a_k^j given in (28), into (33) leads to

$$\begin{aligned} \left(\frac{\partial}{\partial r} + \frac{1}{r} - \frac{1}{c} \frac{\partial}{\partial t} \right) w_{nm}^j &= -\frac{j(j-1) - n(n+1)}{r^2} \sum_{k=j-1}^{n} a_{j-1}^k r^{-k-j} \, \phi_{nm}^k \\ &= -\frac{j(j-1) - n(n+1)}{r^2} \, w_{nm}^{j-1} \end{aligned} \tag{34}$$

Using this key result in (32) defines the following recursive sequence for the functions $w_{nm}^j(r,t)$, $j = 1, 2, \ldots, p_n$

$$\frac{1}{c} \frac{\partial w_{nm}^j}{\partial t} = \frac{j(j-1) - n(n+1)}{2r^2} \, w_{nm}^{j-1} - \frac{j}{r} w_{nm}^j + \frac{1}{2} w_{nm}^{j+1} \tag{35}$$

with $w_{nm}^0 = \phi_{nm}$, and $w_{nm}^{p_n+1} = 0$.

Rescaling the variables by 2^{1-j}, applying the spherical harmonic expansion to (29) and (35), and making use of (12), we rederive the sequence of local radiation boundary conditions involving tangential derivatives given by Hagstrom and Hariharan [19]

$$\left(\frac{1}{c} \frac{\partial}{\partial t} + \frac{\partial}{\partial r} + \frac{1}{r} \right) \phi = v_1 \tag{36}$$

$$\left(\frac{1}{c} \frac{\partial}{\partial t} + \frac{j}{r} \right) v_j = \frac{1}{4r^2} (j(j-1) + \Delta_\Gamma) v_{j-1} + v_{j+1} \tag{37}$$

where

$$v_j(r, \theta, \varphi, t) = 2^{1-j} \sum_{n \geqslant 0} \sum_{|m| \leqslant n} w_{nm}^j(r,t) \, Y_{nm}(\theta, \varphi) \tag{38}$$

for $j = 1, 2, \ldots, p$, and $v_0 = 2\phi$. With p auxiliary functions $\{v_1, v_2, \ldots, v_p\}$, then $v_{p+1} = 0$, and $B_{p+1} \, \phi = 0$, i.e. the radiation boundary condition (36), together with the sequence of p equations (37), is equivalent to the $p+1$ order Bayliss and Turkel local boundary condition. For

example, if only one auxiliary equation is solved for v_1, then v_2 is set to zero, and the radiation boundary condition is equivalent to the second-order boundary condition $B_2\,\phi = 0$. Furthermore, if the solution ϕ contains only N harmonics, then with $p = N$ auxiliary functions, the radiation boundary condition is exact. This result follows from the finite multipole expansion (15), with the index defined over the finite range $k = 0, 1, \ldots, n$. While these conditions can be effectively implemented in a finite difference scheme [19], direct finite element implementation in a standard Galerkin variational equation would result in a non-symmetric system of equations.

To address this difficulty, we recognize that when evaluated on the artificial boundary at $r = R$, sequence (35) forms a system of first-order ordinary differential equations in time for the auxiliary functions, $v_{nm}^j(t) = 2^{1-j}\, w_{nm}^j(R,t)$. Let $\mathbf{v}_{nm}(t) = \{2^{1-j}\, w_{nm}^j(R,t)\},\ j = 1, 2, \ldots, p_n$, and define a time-dependent vector function of order p_n

$$\mathbf{v}_{nm}(t) = [v_{nm}^1(t), v_{nm}^2(t), \ldots, v_{nm}^{p_n}(t)]^{\mathrm{T}} \tag{39}$$

then the first-order system of equations may be written as a matrix differential equation for each spherical harmonic similar to the Cauchy problem appearing in the Grote and Keller nonreflecting boundary condition [10, 12]

$$\frac{\mathrm{d}}{\mathrm{d}t}\mathbf{v}_{nm}(t) = \mathbf{A}_n\,\mathbf{v}_{nm}(t) + \mathbf{b}_n \phi_{nm}(R,t) \tag{40}$$

Here, the constant $p_n \times p_n$, tri-diagonal matrix $\mathbf{A}_n = \{A_n^{ij}\}$, is defined with band

$$\mathbf{A}_n = \frac{c}{R}\mathsf{B}\left[\frac{i(i-1) - n(n+1)}{4R}, -i, R\right] \tag{41}$$

i.e.

$$A_n^{ij} = \frac{c}{R}\begin{cases} R & \text{if } i = j-1 \\ -i & \text{if } i = j \\ [i(i-1) - n(n+1)]/4R & \text{if } i = j+1 \\ 0 & \text{otherwise} \end{cases} \tag{42}$$

The constant vector $\mathbf{b}_n = \{b_n^j\}$ is defined by

$$\mathbf{b}_n = -\frac{n(n+1)c}{2R^2}\mathbf{e}_1 \tag{43}$$

where $\mathbf{e}_1$ is the unit vector

$$\mathbf{e}_1 = [1, 0, \ldots, 0]^{\mathrm{T}} \tag{44}$$

We then define our reformulated boundary condition by taking the spherical harmonic expansion of (29), i.e. multiplying by Y_{nm}, summing over n and m, and evaluating on the truncation boundary at $r = R$

$$\left(\frac{1}{c}\frac{\partial}{\partial t} + \frac{\partial}{\partial r} + \frac{1}{r}\right)\phi = \sum_{n=1}^{\infty}\sum_{m=-n}^{n} v_{nm}^1(t) Y_{nm}(\theta,\varphi) \quad \text{on } \Gamma \tag{45}$$

where the component $v_{nm}^1(t) = w_{nm}^1(R,t)$ satisfies the Cauchy problem for each harmonic defined by the first-order matrix system (40), with initial condition $\mathbf{v}_{nm}(0) = 0$, and driven by the radial

modes defined by the spherical harmonic transform

$$\phi_{nm}(R,t) = \int_0^{2\pi} \int_0^{\pi} Y^*_{nm}(\theta,\varphi)\, \phi(R,\theta,\varphi,t)\, \sin\,\theta\, \mathrm{d}\theta\, \mathrm{d}\varphi \tag{46}$$

Here, the asterisk indicates complex conjugate.

We note that when the number of functions $v^j_{nm}(t) = 2^{1-j} w^j_{nm}(R,t)$ included in the system (40) is equal to the number of angular harmonics in the solution, i.e. $p_n = n$, for $n = 1, 2, \ldots, \infty$, then $v^{n+1}_{nm}(t) = 0$, and the boundary condition is exact and equivalent to the exact Non-Reflecting Boundary Condition (NRBC) first derived in Reference [10] with improved scaling in Reference [12]. We use the term *exact* to define a unique solution which, for all $t > 0$, coincides with the restriction to Ω of the solution of the original problem posed on the unbounded domain $\mathscr{R}$.

The auxiliary functions in (40) satisfy the property, $v^{j+1}_{nm} = O(R^{-2}) v^j_{nm}$, so that $v^{j+1}_{nm} < v^j_{nm}$, and $v^j_{nm} = O(R^{-2j-1})$. Thus for accurate solutions, it is sufficient to use a radial modal order which is less than the angular modal order, i.e. $p_n < n$. In this case the boundary condition (45) forms a *uniform asymptotic approximation* to the exact condition. For a fixed number P, and $p_n = P$, for $n \geqslant P$, and $p_n = n$, for $n < P$, then the radiation boundary condition defined in terms of spherical harmonics given in (45) and (65) is equivalent to the local sequence given in (36) with P auxiliary equations defined by (37).

In computation, the infinite sum over n in (45) is truncated at a finite value N

$$B_1\phi = \sum_{n=1}^{N} \sum_{|m| \leqslant n} v^1_{nm}(t)\, Y_{nm}(\theta,\varphi), \quad n \leqslant N \tag{47}$$

with remainder $B_1\phi = 0$ for $n > N$. Use of (47) with $p_n = n$, on a spherical boundary Γ will exactly represent all harmonics ϕ_{nm}, for $n \leqslant N$. For $n > N$, the truncated condition (47) approximates the harmonics with the local operator $B_1\phi = 0$, with leading error of order $O(1/R^3)$. We note that the memory needed to store the function v^1_{nm} for use in Equation (47) is equal to $N_\mathrm{T} - 1$, where $N_\mathrm{T} = (N+1)^2$ is the total number of harmonics in the truncated solution.

In the following we denote the truncated boundary condition (47) by RBC1(N,P), where N defines the number of terms included in the truncated series, and $P \leqslant N$ defines the maximum number of equations, included in the Cauchy problem (40), i.e. $P = \{\max(p_n),\ p_n \leqslant n\}$, for each mode $n \leqslant N$, indexed by $|m| \leqslant n$. In particular, we define the number of equations $p_n \in \mathscr{P}$, used in (40), for each mode $n \leqslant N$, from the following conditions:

$$\mathscr{P} = \{\, p_n \in \mathbb{Z} \mid p_n = n \text{ for } n < P \text{ and } p_n = P \text{ for } n \geqslant P\} \tag{48}$$

If the solution contains only N angular harmonics, and with $p_n \in \mathscr{P}$, then RBC1(N,P) is equivalent to the Hagstrom and Hariharan condition (36) defined by the sequence of equations (37). With $p_n \in \mathscr{P}$, the total number of auxiliary equations for v^j_{nm} is order $O(P N^2)$, in particular

$$N_p = \sum_{n=1}^{P} n(2n+1) + \sum_{n=P+1}^{N} P(2n+1) = \frac{1}{6} P(5 + 12N + 6N^2 - 3P + 2P^2) \tag{49}$$

The work per step and storage associated with the radiation boundary condition is proportional to N_p.

In general, do to the rapid convergence of the functions $v^{j+1}_{nm} = O(R^{-2}) v^j_{nm}$, then $P \ll N$ is sufficient for accurate solutions, with corresponding reduction in storage and work. When $P = N$, the

boundary condition RBC1(N,N) is exact for modes $n \leqslant N$, with $O(R^{-3})$ error for modes $n>N$. For the exact condition, the total number of auxiliary equations increases to order $O(N^3)$

$$N_p = \sum_{n=1}^{N} n(2n+1) = \frac{1}{6}N(5+9N+4N^2) \tag{50}$$

3.1. Alternative scaling of auxiliary functions

Alternatively, let $y_{nm}^j = R^j v_{nm}^j$, then the sequence (35) becomes

$$\frac{R}{c}\frac{\mathrm{d}}{\mathrm{d}t}y_{nm}^j = \frac{j(j-1)-n(n+1)}{4}\, y_{nm}^{j-1} - j\, y_{nm}^j + y_{nm}^{j+1} \tag{51}$$

This rescaled system of ordinary differential equations can be written in matrix form as

$$\frac{\mathrm{d}}{\mathrm{d}t}\mathbf{y}_{nm}(t) = \mathbf{B}_n\, \mathbf{y}_{nm}(t) + R\mathbf{b}_n \phi_{nm}(R,t) \tag{52}$$

where y_{nm}^j, $j=1,2,\ldots,p_n$, are the elements of the vector $\mathbf{y}_{nm}$, and $\mathbf{B}_n = \{B_n^{ij}\}$, is a $p_n \times p_n$, *normalized* tri-diagonal matrix with band

$$\mathbf{B}_n = \frac{c}{R}\mathsf{B}\left[\frac{(n+i)(i-n-1)}{4}, -i, 1\right] \tag{53}$$

With this modification to the radiation boundary condition, the normalized coefficient matrix is independent of R, and the eigenvalues of the system may be readily computed.

3.2. Modified radiation boundary condition

To improve the approximation to the truncated harmonics $n>N$, without affecting the modes $n \leqslant N$, we define a modified boundary condition using (26) for $j=1$, and $r=R$, i.e. applying the second-order Bayliss and Turkel operator, with remainder

$$B_2\phi_{nm}(R,t) = 2v_{nm}^2(t) \tag{54}$$

we form the inverse spherical harmonic transform with the result

$$B_2\phi = \sum_{n=2}^{\infty}\sum_{m=-n}^{n} 2v_{nm}^2(t)Y_{nm}(\theta,\varphi) \quad \text{on } \Gamma \tag{55}$$

where the function $v_{nm}^2(t) = w_{nm}^2(R,t)/2$ satisfies the same first-order matrix system (40), for each harmonic (46). In practice, the sum over n in (55) is truncated at a finite value N. For $n>N$, the truncated condition (55) reduces to $B_2\phi = 0$ on Γ. This condition approximates the harmonics $n>N$, with leading error $O(1/R^5)$. Therefore, when truncated at a finite value N, the boundary condition (55) approximates the modes $n>N$ with greater accuracy than (45).

Following the steps given in Reference [13], Equation (55) can be implemented in a symmetric finite element variational equation similar to that used for the modified non-reflecting boundary condition given in Reference [11]. In this case, we introduce additional auxiliary functions $q_{nm}(t)$ and $\psi(\theta,\varphi,t)$, such that

$$B_1\phi - \frac{1}{2R}\Delta_\Gamma\psi = R\sum_{n=2}^{\infty}\sum_{m=-n}^{n} q_{nm}(t)Y_{nm} \quad \text{on } \Gamma,\ t \geqslant 0 \tag{56}$$

$$\left(\frac{R}{c}\frac{\partial}{\partial t}+1\right)\Delta_\Gamma[\psi]=\Delta_\Gamma[\phi],\quad \psi(\theta,\varphi,0)=0 \tag{57}$$

$$\left(\frac{R}{c}\frac{\mathrm{d}}{\mathrm{d}t}+1\right)q_{nm}(t)=v_{nm}^2(t),\qquad q_{nm}(0)=0 \tag{58}$$

The three equations (56)–(58), define an equivalent form of the radiation boundary condition (55), suitable for implementation in a symmetric finite element formulation, see References [13, 14].

3.3. Grote and Keller non-reflecting boundary conditions

In this section we rederive the exact NRBC formulated in References [10, 12], directly from the multipole expansion (15) and recursion relation (16). Then using a linear transformation, we establish the equivalence between the exact NRBC and RBC1(N,N) defined by (45) and (40) with $p_n=n$.

We begin with the recurrence relation (16) for $k=1$

$$\frac{1}{c}\frac{\partial}{\partial t}\phi_{nm}^1(r-ct)=-c_n^1\phi_{nm}^0(r-ct) \tag{59}$$

where $c_n^1=-n(n+1)/2$. Then replace ϕ_{nm}^0 in (59), using the asymptotic wave expansion (15) with the term $k=0$ written explicitly

$$\phi_{nm}^0(r-ct)=-\sum_{k=1}^{n} r^{-k}\,\phi_{nm}^k(r-ct)+r\,\phi_{nm}(r,t) \tag{60}$$

with the result

$$\frac{1}{c}\frac{\partial}{\partial t}\phi_{nm}^1(r-ct)=c_n^1\sum_{k=1}^{n} r^{-k}\,\phi_{nm}^k(r-ct)-rc_n^1\,\phi_{nm}(r,t) \tag{61}$$

Defining the scaled wave function

$$z_{nm}^k(t)=-\frac{1}{c_n^1R^k}\phi_{nm}^k(R-ct) \tag{62}$$

then (61), evaluated on the boundary $r=R$, can be written as a first-order ordinary differential equation in time driven by radial harmonics on the spherical boundary

$$\frac{\mathrm{d}}{\mathrm{d}t}z_{nm}^1(t)=c_n^1\frac{c}{R}\sum_{k=1}^{n} z_{nm}^k(t)+c\,\phi_{nm}(R,t) \tag{63}$$

Similarly, using the change of variable (62), the recursion relation (16) evaluated at $r=R$, gives the sequence of equations for $k=2,3,\ldots,n$

$$\frac{\mathrm{d}}{\mathrm{d}t}z_{nm}^k(t)=-c_n^k\frac{c}{R}z_{nm}^{k-1}(t) \tag{64}$$

where c_n^k is defined in (17). Writing (63) and (64) in matrix form, we derive the same first-order system of auxiliary equations first derived in Reference [10] with improved scaling in Reference [12]

$$\frac{\mathrm{d}}{\mathrm{d}t}\mathbf{z}_{nm}(t)=\mathbf{C}_n\,\mathbf{z}_{nm}(t)+c\,\phi_{nm}(R,t)\mathbf{e}_1 \tag{65}$$

Here $\{z_{nm}^j\}$, $j=1,2,\ldots,n$, are the components of the time-dependent vector $\mathbf{z}_{nm}(t)$, with $n\times n$ coefficient matrix

$$\mathbf{C}_n=\frac{c}{R}\begin{bmatrix} \dfrac{-n(n+1)}{2} & \dfrac{-n(n+1)}{2} & \cdots & \dfrac{-n(n+1)}{2} & \dfrac{-n(n+1)}{2} \\ \dfrac{(n+2)(n-1)}{2\times 2} & 0 & \cdots & 0 & 0 \\ 0 & \dfrac{(n+3)(n-2)}{2\times 3} & \cdots & 0 & 0 \\ \vdots & \vdots & \ddots & \vdots & \vdots \\ 0 & 0 & \cdots & 1 & 0 \end{bmatrix} \tag{66}$$

defined with coefficients

$$C_n^{ij}=\frac{c}{R}\begin{cases} \dfrac{-n(n+1)}{2} & \text{if } i=1 \\ \dfrac{(n+i)(n-i+1)}{2i} & \text{if } i=j+1 \\ 0 & \text{otherwise} \end{cases} \tag{67}$$

Using the scaling (62), in (20) and (21), evaluated at $r=R$, the residual $v_{nm}^1(t)$, of the local B_1 operator acting on the radial wave expansion (15) may be expressed in terms of a linear combination of $z_{nm}^k(t)$

$$v_{nm}^1(t)=\frac{c_n^1}{R^2}\sum_{k=1}^{n} k\, z_{nm}^k(t)=\mathbf{e}_n\cdot\mathbf{z}_{nm}(t) \tag{68}$$

where $\mathbf{e}_n=\{e_n^k\}$ is a vector with coefficients

$$e_n^k=-\frac{n(n+1)k}{2R^2},\quad k=1,2,\ldots,n \tag{69}$$

and z_{nm}^k represent scaled wave functions.

With the residual expressed in terms of the wave function expansion (68) and taking the spherical harmonic expansion of the first-order condition (20) we rederive the nonreflecting boundary condition given in References [10, 12]

$$\left(\frac{1}{c}\frac{\partial}{\partial t}+\frac{\partial}{\partial r}+\frac{1}{r}\right)\phi=\sum_{n=1}^{\infty}\sum_{m=-n}^{n}\mathbf{e}_n\cdot\mathbf{z}_{nm}(t)\,Y_{nm}(\theta,\varphi)\quad\text{on }\Gamma \tag{70}$$

where $\mathbf{z}_{nm}(t)$ satisfies (65).

Our derivation of (70) and (65), based on the radial asymptotic (multipole) expansion (15) is relatively straightforward and provides a physical interpretation of the auxiliary functions $z_{nm}^k(t)$. Here the vector function $\mathbf{z}_{nm}(t)$ satisfies the auxiliary equations (65), with components defined by the scaled radial wave functions appearing in the multipole expansion for ϕ_{nm}. The first equation in system (65) represents the multipole expansion for the radial modes in terms of scaled wave functions, while the remaining equations are equivalent to the associated recursion equation for the wave functions. As a result, the matrix $\mathbf{C}_n$ is not banded and has zeros on the diagonal except for the first. Since the multipole expansion involves a summation of wave functions

from $k=1,2,\ldots,n$, all of the wave functions z_{nm}^k must be included in the system of auxiliary equations (65).

We note several distinct advantages of the formulation (45) compared to (70), including:

(i) The radiation boundary condition (45) avoids the inner product $\mathbf{c}_n \cdot \mathbf{z}_{nm}$ required to form the residual of the B_1 operator in (41).
(ii) The full system matrix $\mathbf{C}_n$ appearing in (66) is replaced by a banded tri-diagonal matrix in (41).
(iii) Since the functions $\mathbf{v}_{nm}(t)$ appearing in (45) and (40) represent residuals of the radial asymptotic expansion with the property $v_{nm}^{j+1} < v_{nm}^j$, and $v_{nm}^j = O(R^{-2j-1})$, then the radial and transverse modal orders of the asymptotic form of RBC1(N,P) may be varied separately with $P<N$. By allowing the number of equations p_n, in system (40), to be less than n, the storage and cost is reduced accordingly.

To establish the equivalence of RBC1(N,N) defined in (45) with (40) or (52) and $p_n=n$, to the exact NRBC defined in (70) with (65), we first determine the relationship between functions $w_{nm}^j(R,t)$ and $z_{nm}^j(t)$. Here the residual of the B_j local operator acting on the radial harmonics ϕ_{nm} given in (27), evaluated at $r=R$, is rewritten in terms of the scaled wave functions z_{nm}^k, using (62)

$$w_{nm}^j(R,t) = \frac{n(n+1)}{2} R^{-j-1} \sum_{k=j}^{n} a_k^j \, z_{nm}^k(t) \tag{71}$$

Then using the scaling $y_{nm}^j(t) = R^j \, v_{nm}^j(t) = R^j 2^{1-j} w_{nm}^j(R,t)$, we have for $j=1,2,\ldots,n$

$$y_{nm}^j(t) = \frac{n(n+1)}{2^j R} \sum_{k=1}^{n} a_k^j \, z_{nm}^k(t) \tag{72}$$

From the above, we see that y_{nm}^j may be viewed as a linear combination of z_{nm}^k. Written in matrix form we define the linear transformation $Q_n(\mathbf{z}_{nm})$ by the matrix-vector product

$$\mathbf{y}_{nm}(t) = \mathbf{Q}_n \, \mathbf{z}_{nm}(t) \tag{73}$$

with $Q_n = \{Q_n^{ij}\}$, defined by the $n \times n$ upper triangular matrix

$$\mathbf{Q}_n = \frac{n(n+1)}{R} \begin{bmatrix} \dfrac{a_1^1}{2} & \dfrac{a_2^1}{2} & \cdots & \dfrac{a_n^1}{2} \\ 0 & \dfrac{a_2^2}{2^2} & \cdots & \dfrac{a_n^2}{2^2} \\ 0 & 0 & \ddots & \vdots \\ 0 & 0 & \cdots & \dfrac{a_n^n}{2^n} \end{bmatrix} \tag{74}$$

Using the linear transformation (73) in the first-order system (52) with $p_n=n$ gives

$$\frac{\mathrm{d}}{\mathrm{d}t} \mathbf{Q}_n \, \mathbf{z}_{nm}(t) = \mathbf{B}_n \mathbf{Q}_n \, \mathbf{z}_{nm}(t) + R \, \mathbf{b}_n \phi_{nm}(R,t) \tag{75}$$

Then multiplying by $\mathbf{Q}_n^{-1}$ gives the equivalent system (65), with coefficient arrays (67) computed from

$$\mathbf{C}_n = \mathbf{Q}_n^{-1}\mathbf{B}_n\,\mathbf{Q}_n, \quad \mathbf{e}_1 = \frac{R}{c}\mathbf{Q}_n^{-1}\mathbf{b}_n \tag{76}$$

The equivalence of system (40) follows from the scaling $y_{nm}^j = R^j v_{nm}^j$.

3.4. Stability

The stability of the ordinary differential equation (40) or equivalently (52) is determined by the eigenvalues of the matrix $\mathbf{B}_n$. For $p_n = n$ the eigenvalues of $\mathbf{B}_n$ are equivalent to the roots of $\mathbf{C}_n$. The eigenvalues λ_n, for $\mathbf{C}_n$ may be determined from the eigensystem

$$(\mathbf{C}_n - \lambda_n\mathbf{I})\,\mathbf{z}_{nm} = \mathbf{0} \tag{77}$$

In Reference [12], we verified numerically that the eigenvalues (roots) of $\mathbf{C}_n$, lie strictly in the left half of the complex plane up to $n \leqslant 75$. Since the maximum real part of the eigenvalues are negative, in fact, $\max(\mathrm{Re}[\lambda_n]) < -1$, solutions to the first-order system of equations for the auxiliary functions are stable. Using the vector transformation (73) in (77) and multiplying by $\mathbf{Q}_n$, gives

$$(\mathbf{B}_n - \lambda_n\mathbf{I})\,\mathbf{y}_{nm} = \mathbf{0} \tag{78}$$

where $\mathbf{B}_n$ is defined in (76). Since the same roots λ_n appear in both (77) and (78), the eigenvalues for the matrices $\mathbf{C}_n$ and $\mathbf{B}_n$, with $p_n = n$, are identical.

To check that the eigenvalues of $\mathbf{B}_n$ for $p_n < n$ also lie in the left half of the complex plane, we compute the maximum real part of the roots for $n = 1, 2, \ldots, 20$, with $p_n = 1, 2, \ldots, n$. In Figure 2, the maximum real part of the eigenvalues of the $p_n \times p_n$ matrices $\mathbf{B}_n$ are plotted as a family of curves for $n = 1, 2, \ldots, 20$, and $p_n \leqslant n$. The values for $p_n < n$ are bounded by the solid curve representing the maximum eigenvalues computed with $p_n = n$. This result implies that both the exact and asymptotic forms of the radiation boundary condition RBC1 are stable.

4. FINITE ELEMENT FORMULATION

In the following, we summarize the finite element formulation for the initial-boundary value problem within the bounded region Ω, supplemented by the radiation boundary condition (45) on Γ. Since both the radiation boundary condition RBC1(N, P) defined in (45) and the closely related NRBC (70), are in the form of the local first-order Bayliss and Turkel operator with residual determined by solving parallel systems of first-order temporal equations, the implementation is similar to that given in References [11, 12]. Extensions for the formulation of the modified condition (55) follows the procedures described in References [13, 14].

4.1. Variational equation

The statement of the weak form for the initial-boundary value problem in the computational domain Ω may be stated as:

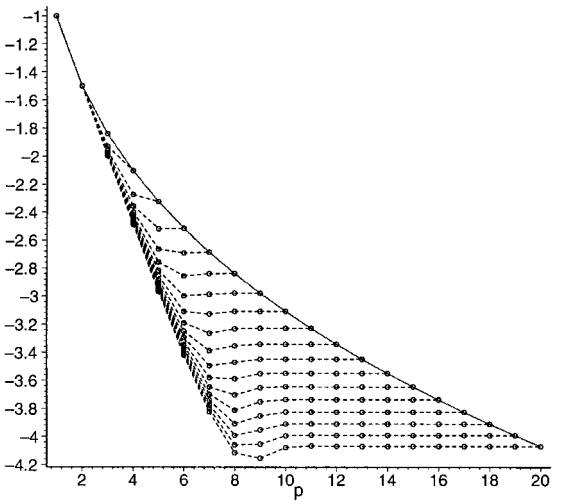

Figure 2. Maximum real part of eigenvalues for the $p_n \times p_n$ matrix $\mathbf{B}_n$ normalized with c/R vs. dimension p_n. The graph shows a family of dashed curves for $n = 1, 2, \ldots, 20$, and $p_n \leqslant n$. The values are bounded by the solid curve representing the maximum eigenvalues computed with $p_n = n$.

Given: $f, \alpha, \beta, \gamma, c$,
Find: $\phi(\mathbf{x}, t)$ in $\Omega \cup \partial\Omega$, such that for all admissible weighting functions $\delta\phi$, the following variational equation is satisfied

$$M(\delta\phi, \phi) + C(\delta\phi, \phi) + K(\delta\phi, \phi) = F_S(\delta\phi) + F_\Gamma(\delta\phi) \tag{79}$$

with

$$M(\delta\phi, \phi) := \int_\Omega \frac{1}{c^2} \delta\phi \, \frac{\partial^2 \phi}{\partial t^2} \mathrm{d}\Omega \tag{80}$$

$$C(\delta\phi, \phi) := \int_{\mathscr{S}} \frac{\beta}{\alpha} \delta\phi \, \frac{\partial \phi}{\partial t} \mathrm{d}\mathscr{S} + \int_\Gamma \frac{1}{c} \delta\phi \, \frac{\partial \phi}{\partial t} \mathrm{d}\Gamma \tag{81}$$

$$K(\delta\phi, \phi) := \int_\Omega \nabla\delta\phi \cdot \nabla\phi \, \mathrm{d}\Omega + \int_{\mathscr{S}} \frac{\gamma}{\alpha} \delta\phi \, \phi \, \mathrm{d}\mathscr{S} + \frac{1}{R} \int_\Gamma \delta\phi \, \phi \, \mathrm{d}\Gamma \tag{82}$$

$$F_S(\delta\phi) := \int_\Omega \delta\phi \, f \, \mathrm{d}\Omega + \int_{\mathscr{S}} \delta\phi \, \frac{g}{\alpha} \mathrm{d}\mathscr{S} \tag{83}$$

$$F_\Gamma(\delta\phi) := \sum_{n=1}^{\infty} \sum_{m=-n}^{n} v_{nm}^1 \int_\Gamma \delta\phi \, Y_{nm} \, \mathrm{d}\Gamma \tag{84}$$

In the above, $v_{nm}^1(t)$ is a component of the vector function $\mathbf{v}_{nm}(t)$ satisfying the system of first-order differential equations (40), driven by the modes $\phi_{nm}(R, t)$ computed from the spherical harmonic transform of ϕ on Γ

$$\frac{\mathrm{d}}{\mathrm{d}t} \mathbf{v}_{nm}(t) = \mathbf{A}_n \, \mathbf{v}_{nm}(t) + \mathbf{b}_n \frac{1}{R^2} \int_\Gamma Y_{nm}^*(\theta, \varphi) \, \phi(R, \theta, \varphi, t) \, \mathrm{d}\Gamma \tag{85}$$

Here $\mathrm{d}\Gamma = R^2 \sin\theta \, \mathrm{d}\theta \, \mathrm{d}\varphi$ for a spherical truncation boundary.

For the scattering problem, a known incident wave $\phi^{(\mathrm{i})}(\mathbf{x},t)$ is scattered from the surface $\mathscr{S}$. The total solution ϕ, is then the superposition of the incident wave $\phi^{(\mathrm{i})}$ and scattered field $\phi^{(\mathrm{s})}$, i.e. $\phi=\phi^{(\mathrm{i})}+\phi^{(\mathrm{s})}$. The scattered field is a solution to the wave equation subject to the radiation boundary condition (45) and condition (3)

$$\alpha\frac{\partial\phi^{(\mathrm{s})}}{\partial n}+\beta\frac{\partial\phi^{(\mathrm{s})}}{\partial t}+\gamma\phi^{(\mathrm{s})}=g_{\mathrm{s}}(\mathbf{x},t),\quad \mathbf{x}\in\mathscr{S},\quad t\in[0,T] \tag{86}$$

where

$$g_{\mathrm{s}}(\mathbf{x},t)=g-\alpha\frac{\partial\phi^{(\mathrm{i})}}{\partial n}-\beta\frac{\partial\phi^{(\mathrm{i})}}{\partial t}-\gamma\phi^{(\mathrm{i})} \tag{87}$$

For a given $\phi^{(\mathrm{i})}$, the scattered field may be solved within Ω using the weak form of the IBVP defined in (79), with ϕ and g replaced with $\phi^{(\mathrm{s})}$ and g_{s}, respectively. We note that this solution requires normal derivatives of the time-dependent incident wave, $\partial\phi^{(\mathrm{i})}/\partial n$, appearing in (87). For complex surfaces, the computation of normal derivatives may be inconvenient.

An alternative formulation which avoids explicitly computing derivatives on $\mathscr{S}$ is derived by exploiting the separable form of the spherical radiation boundary and solving for the total field ϕ. In order to directly solve ϕ within Ω, the variational equation is modified to represent the incident wave field on the radiation boundary Γ. The scattered field is then computed by subtracting the given incident wave from the total field, i.e. $\phi^{(\mathrm{s})}=\phi-\phi^{(\mathrm{i})}$. To solve for the total field, we modify the linear operator F_Γ as

$$F_\Gamma(\delta\phi):=\sum_{n=1}^{\infty}\sum_{m=-n}^{n}v_{nm}^{1}\int_\Gamma\delta\phi\,Y_{nm}\,\mathrm{d}\Gamma+\int_\Gamma\delta\phi\,B_1\,\phi^{(\mathrm{i})}\,\mathrm{d}\Gamma \tag{88}$$

where

$$B_1=\left(\frac{\partial}{\partial r}+\frac{1}{c}\frac{\partial}{\partial t}+\frac{1}{r}\right) \tag{89}$$

is the first-order local operator of Bayliss and Turkel, and $v_{nm}^{1}(t)$ is a solution of the first-order system

$$\frac{\mathrm{d}}{\mathrm{d}t}\mathbf{v}_{nm}(t)=\mathbf{A}_n\,\mathbf{v}_{nm}(t)+\mathbf{b}_n\,\phi_{nm}^{(\mathrm{s})}(R,t) \tag{90}$$

driven by modes

$$\phi_{nm}^{(\mathrm{s})}(R,t)=\frac{1}{R^2}\int_\Gamma Y_{nm}^{*}(\theta,\varphi)\,[\phi(R,\theta,\varphi,t)-\phi^{(\mathrm{i})}(R,\theta,\varphi,t)]\,\mathrm{d}\Gamma \tag{91}$$

In this formulation, normal derivatives of the incident wave are not computed on the surface $\mathscr{S}$. Instead, the incident wave is represented on the spherical radiation boundary Γ, where the normal derivative reduces to the radial derivative, $\partial\phi^{(\mathrm{i})}/\partial n=\partial\phi^{(\mathrm{i})}/\partial r$, which is easily computed.

4.2. Finite element discretization

To obtain a finite element approximation to the solution of the variational equation (79), the domain $\bar{\Omega}$ is discretized into a finite number of subdomains (elements), and we apply the standard

Galerkin semi-discrete approximation

$$\phi(\mathbf{x},t) \approx \phi^h(\mathbf{x},t) = \mathbf{N}(x)\,\boldsymbol{\phi}(t) \tag{92}$$

$$\delta\phi(\mathbf{x},t) \approx \delta\phi^h(\mathbf{x},t) = \mathbf{N}(x)\,\delta\boldsymbol{\phi}(t) \tag{93}$$

where $\mathbf{N}(\mathbf{x})$ is a row vector array of standard C^0 basis functions with compact support associated with each node, and $\boldsymbol{\phi}(t)$ is a time-continuous column vector containing the nodal values of ϕ^h. The superscript h denotes a finite-dimensional basis. Using this approximation in (79), we arrive at the following system of second-order ordinary differential equations in time

$$\mathbf{M}\ddot{\boldsymbol{\phi}}(t) + \mathbf{C}\dot{\boldsymbol{\phi}}(t) + \mathbf{K}\boldsymbol{\phi}(t) = \mathbf{F}(t), \quad t > 0 \tag{94}$$

$$\boldsymbol{\phi}(0) = \boldsymbol{\phi}_0, \quad \dot{\boldsymbol{\phi}}(0) = \dot{\boldsymbol{\phi}}_0 \tag{95}$$

In the above, $\mathbf{M}$, $\mathbf{C}$, and $\mathbf{K}$ are standard arrays associated with the discretization of the wave equation and the local B_1 operator; and $\mathbf{F}(t) = \mathbf{F}_S + \mathbf{F}_\Gamma$ is the discrete force vector composed of a standard load vector $\mathbf{F}_S$ and a part associated with the auxiliary functions appearing in the radiation boundary condition. In practice, for real boundary condition data on $\mathscr{S}$, it is advantageous to use real instead of complex spherical harmonics. In this case the spherical harmonic is given by the real and imaginary parts of (10) with a modified normalization. Using real values, we define the even and odd harmonics as

$$Y^{\mathrm{c}}_{nm} := P^m_n(\cos\theta)\,\cos m\varphi \tag{96}$$

$$Y^{\mathrm{s}}_{nm} := P^m_n(\cos\theta)\,\sin m\varphi \tag{97}$$

so that the force vector takes the form

$$\mathbf{F}_\Gamma(t) = \sum_{n=1}^{N} {\sum_{m=0}^{n}}' [\, v^{\mathrm{c}}_{nm,1}(t)\mathbf{f}^{\mathrm{c}}_{nm} + v^{\mathrm{s}}_{nm,1}(t)\mathbf{f}^{\mathrm{s}}_{nm}] \tag{98}$$

where the prime on the sum indicates that a factor of 1/2 multiplies the term with $m = 0$, and

$$\mathbf{f}^{\mathrm{c}}_{nm} := \int_\Gamma \mathbf{N}^{\mathrm{T}}(\theta,\varphi)\, Y^{\mathrm{c}}_{nm}(\theta,\varphi)\,\mathrm{d}\Gamma \tag{99}$$

$$\mathbf{f}^{\mathrm{s}}_{nm} := \int_\Gamma \mathbf{N}^{\mathrm{T}}(\theta,\varphi)\, Y^{\mathrm{s}}_{nm}(\theta,\varphi)\,\mathrm{d}\Gamma \tag{100}$$

In (98), the functions $v^{\mathrm{c}}_{nm,1}$ and $v^{\mathrm{s}}_{nm,1}$ are the first element of the vector arrays $\mathbf{v}^{\mathrm{c}}_{nm} = \{v^{\mathrm{c}}_{nm,j}\}$, and $\mathbf{v}^{\mathrm{s}}_{nm} = \{v^{\mathrm{s}}_{nm,j}\}$, which satisfy the system of first-order differential equations (40) driven by the even and odd radial modes at $r = R$

$$\phi^{\mathrm{c}}_{nm}(R,t) = \frac{2}{R^2 N_{nm}}\,\mathbf{f}^{\mathrm{cT}}_{nm}\,\boldsymbol{\phi}_\Gamma(t) \tag{101}$$

$$\phi^{\mathrm{s}}_{nm}(R,t) = \frac{2}{R^2 N_{nm}}\,\mathbf{f}^{\mathrm{sT}}_{nm}\,\boldsymbol{\phi}_\Gamma(t) \tag{102}$$

In the above, $\boldsymbol{\phi}_\Gamma(t) = \{\phi_I(t)\}$, $I = 1,2,\ldots,N_\Gamma$, is a vector of nodal solutions on the artificial boundary Γ with N_Γ nodes.

The sum over n is truncated at a finite value N. For $N = 0$, the formulation reduces to the B_1 local boundary condition. For $N \geqslant 1$, the radiation boundary condition only requires inner products

of spherical harmonics and finite element basis functions with compact support within the boundary vector $\mathbf{f}_{nm}$. As a result, the components of the force vector are easy to compute, either at each node on the radiation boundary Γ, or over each element on the boundary and using standard element vector assembly. We note that the implementation does not disturb in any way the symmetric, and banded/sparse structure of the finite element matrix equations.

Furthermore, we note that the harmonics $Y_{nm}(\theta,\varphi)$ may be approximated by a projection onto the finite-dimensional basis. In particular, the harmonics may be approximated by the interpolant of Y_{nm}, using the expansions

$$Y^{\mathrm{c}}_{nm}(\theta,\varphi)\approx \mathbf{N}(\theta,\varphi)\,\mathbf{y}^{\mathrm{c}}_{nm} \tag{103}$$

$$Y^{\mathrm{s}}_{nm}(\theta,\varphi)\approx \mathbf{N}(\theta,\varphi)\,\mathbf{y}^{\mathrm{s}}_{nm} \tag{104}$$

where $\mathbf{y}_{nm}=\{Y_{nm,l}\},\ l=1,2,\ldots,N_\Gamma$, is a vector containing the nodal values of the harmonic defined by (n,m) on Γ, i.e. $y_{nm,l}=Y_{nm}(\theta_l,\varphi_l)$.

Using this expansion in (98) we have

$$\mathbf{F}_\Gamma(t)=\sum_{n=1}^{N}{\sum_{m=0}^{n}}'\mathbf{M}_\Gamma[\mathbf{y}^{\mathrm{c}}_{nm}\,v^{\mathrm{c}}_{nm,1}(t)+\mathbf{y}^{\mathrm{s}}_{nm}\,v^{\mathrm{s}}_{nm,1}(t)] \tag{105}$$

where $v^{\mathrm{c}}_{nm,1}$ and $v^{\mathrm{s}}_{nm,1}$ are driven by

$$\phi^{\mathrm{c}}_{nm}(R,t)\;=\;\frac{2}{R^2N_{nm}}\,\mathbf{y}^{\mathrm{cT}}_{nm}\,\mathbf{M}_\Gamma\,\boldsymbol{\phi}_\Gamma(t) \tag{106}$$

$$\phi^{\mathrm{s}}_{nm}(R,t)\;=\;\frac{2}{R^2N_{nm}}\,\mathbf{y}^{\mathrm{sT}}_{nm}\,\mathbf{M}_\Gamma\,\boldsymbol{\phi}_\Gamma(t) \tag{107}$$

In the above, $\mathbf{M}_\Gamma$ is the $N_\Gamma\times N_\Gamma$ symmetric matrix

$$\mathbf{M}_\Gamma:=\int_\Gamma \mathbf{N}^{\mathrm{T}}\,\mathbf{N}\,\mathrm{d}\Gamma \tag{108}$$

We note that this matrix may be diagonalized using nodal (Lobatto) quadrature, so that the matrix-vector multiply is reduced to an inner product.

Let N_Γ denote the number of grid points on the truncating surface Γ, and $N_{\mathrm{T}}=(N+1)^2$, the total number of harmonics included in the radiation boundary condition. For typical problems, $N_{\mathrm{T}}\ll N_\Gamma$, so that the extra work computing the spherical transforms is relatively small. To compute the inner products, it is not necessary to compute N_{T} inner products over the entire sphere. Since the spherical harmonics Y_{nm} separate in θ and φ, it is sufficient to compute $O(N)$ inner projects in φ, and then to compute $O(N^2)$ one-dimensional inner products in θ. If a large number of harmonics N_{T} are needed such that $N_{\mathrm{T}}\approx N_\Gamma$, then the work required can be reduced by an order of magnitude using a simple separation of variables and Fast Fourier Transform (FFT) for the variables φ [30]. On a grid of $2N$ points equispaced in φ by N Gaussian nodes in $\cos\theta$ the work can be reduced further using recently developed fast spherical transform algorithms, e.g. References [31, 32], with work reduced to order $O(N_{\mathrm{T}}\ln N_{\mathrm{T}})$, and $O(N_{\mathrm{T}}\ln^2 N_{\mathrm{T}})$, respectively.

As discussed in Reference [12], one time-integration approach is to apply the central difference method directly to (94). This explicit method requires only the forcing term $\mathbf{F}^k=\mathbf{F}(t_K)$ at time step $t_K=k\,\Delta t$. Therefore, to update the solution $\mathbf{d}^{k+1}=\boldsymbol{\phi}(t_{k+1})$, only the evaluation of $\mathbf{v}^k_{nm}=\mathbf{v}_{nm}(t_K)$ is needed. To numerically solve (40), either the explicit second-order Adams–Bashforth method or the

implicit second-order Adams–Moulton method (trapezoidal rule) may be used. The computational work required in solving is negligible, since the matrices $\mathbf{A}_n$, are banded, relatively small (usually $N \leqslant 25$), and remain constant. When $p_n < n$, the work is further reduced.

An alternative approach is to apply the Newmark family of algorithms (and variations such as HHT-α) in predictor/corrector form to the semidiscrete equations (94), see Reference [12]. Any of the members of the Newmark family may be used, including the second-order accurate and unconditionally stable trapezoidal rule, and conditionally stable central difference method. When solving using the explicit central difference method, the equations may be decoupled using standard diagonal mass $\mathbf{M}$, and damping matrices $\mathbf{C}$, e.g. using nodal quadrature, row-sum technique, or the HRZ lumping scheme. The solution of the Newmark algorithm requires that the forcing term $\mathbf{F}^{k+1}$, and therefore $\mathbf{v}_{nm}^{k+1}$ be available. In this case the value $\mathbf{v}_{nm}^{k+1}$, may be computed concurrently using an explicit time integrator applied to (40); e.g. the explicit second-order accurate Adams–Bashforth algorithm. Complete algorithms for computing the solution concurrently with auxiliary functions on Γ, using either implicit or explicit time integrators, are given in Reference [12].

5. NUMERICAL STUDIES

Numerical studies are performed to study the accuracy and convergence properties of the exact and asymptotic form of the radiation boundary condition RBC1(N,P) defined in (45) and (40). In the first example we investigate the ability of RBC1(N,P) to accurately represent multipole solutions on Γ. In the second example, we investigate a challenging problem of steady state radiation from a piston on a sphere involving an infinite number of harmonics. Next, numerical studies are performed using the total field formulation for scattering from a rigid sphere. In the final example we study fully transient solutions for a circular piston transducer mounted in an infinite rigid planar baffle. For each problem, comparisons are made to numerical solutions using the local boundary operators B_1 and B_2, and analytical solutions.

5.1. Spherical harmonic radiation

Consider time-dependent multipole radiation from a sphere of radius $a = 1$, driven by

$$\phi(a,\theta,t) = P_n(\cos\theta)\,\sin\omega t\,H(t), \quad 0 \leqslant \theta \leqslant \pi \tag{109}$$

where $H(t)$ is the unit step (Heaviside) function.

The exact steady state solution for this problem is

$$\phi(r,\theta,t) = -\,\mathrm{Imag}\left\{\frac{h_n(kr)}{h_n(ka)}\,P_n(\cos\theta)\mathrm{e}^{-\mathrm{i}\omega t}\right\}, \quad r \geqslant a \tag{110}$$

In the above, P_n are Legendre polynomials, h_n are spherical Hankel functions of the first kind, and $k = \omega/c$ is the wave number. Closed-form transient solutions for modes $n = 0$ and $n = 1$ are available by exact evaluation of a Laplace transform. For general problems, when the number of equations used in (40) is equal to the mode number, $p_n = n$, then the radiation boundary condition RBC1(N,N), is exact for modes $n \leqslant N$. For multipole radiation defined by (109), the solution involves only a single mode n. In this case, setting RBC1$(N,0)$ with $N = n$, is equivalent to the first-order local Bayliss and Turkel condition B_1. This condition is exact for the 'breathing' mode corresponding to $n = 0$ in (109) yet only approximates higher modes. Similarly, the second-order

local condition B_2 is equivalent to the asymptotic radiation condition RBC1$(N,1)$, $N = n$, which is exact for the first two modes corresponding to $n = 0$ and $n = 1$.

The problem is axisymmetric and independent of φ. Therefore, it is sufficient to compute the solution in the domain Ω defined by the (r,θ) plane for $a \leqslant r \leqslant R$, and $0 \leqslant \theta \leqslant \pi$. The radiation boundary condition reduces naturally to the axisymmetric problem by setting the index $m = 0$ in (45), with the result

$$B_1[\phi] = -\frac{1}{R}\sum_{n=1}^{\infty} v_{nm,1}(t)\, P_n(\cos\theta) \tag{111}$$

Here the system of equations (65) for $\mathbf{z}_{n0}$ are driven by the radial modes

$$\phi_{n0}|_{r=R} = \frac{(2n+1)}{2}\int_0^{\pi} \phi(R,\theta,t) P_n(\cos\theta)\sin\theta\, \mathrm{d}\theta \tag{112}$$

For this example problem the artificial boundary Γ is set at $R = 2$. The computational domain inside Γ is discretized with a uniform mesh with 20×120 standard 4-node bilinear axisymmetric finite elements (20 evenly spaced elements in $1 \leqslant r \leqslant 2$, and 120 evenly spaced elements in $0 \leqslant \theta \leqslant \pi$). The wave speed is set at $c = 1$ corresponding to a non-dimensional time '$t\ a/c$'. The calculation is driven with mode $n = 6$ and a relatively low frequency $\omega a/c = \pi/4$, corresponding to a steady state wavelength $\lambda/a = 8$. The number grid points per transverse mode on the boundary is $N_\Gamma/N = 20$. A time-harmonic solution is obtained by starting from rest with initial data $\phi_0 = 0$ and $\dot{\phi}_0 = 0$ and driving the solution to steady state with a time step $\Delta t = 0.08$. The finite element equations are solved with the Newmark time-stepping algorithm defined by the trapezoidal rule. The mesh and time increment are relatively small so that the error is primarily due to the radiation boundary treatment.

For reference, contours of the numerical solution using the exact radiation boundary condition RBC1(6,6), after reaching steady state are illustrated in Figure 3. Time-dependent solutions on the radiation boundary Γ, at the pole defined by $R = 2$, and $\theta = 0$, are shown in Figure 4. To study the accuracy of the various boundary treatments, it is sufficient to compare numerical results to the exact steady state solution given in (110) with $n = 6$. Numerical solutions are computed using local operators B_1, and B_2, and the radiation boundary condition RBC1(N,P), with $N = 6$, and $P = N$. The results show that the numerical solution using both B_1 and B_2 exhibits significant amplitude and phase error, indicating spurious reflection from the radiation boundary Γ. As expected, the solution obtained using RBC1(6,6) can barely be distinguished from the exact time-harmonic solution in the steady state interval beyond $t > 5$.

The instantaneous error $e(t) = \phi^h - \phi$, measured in L_2 norm on a spherical boundary with radius $r = R_0$ is defined as

$$E(t) = \left\{\int_0^{\pi} [\phi^h(R_0,\theta,t) - \phi(R_0,\theta,t)]^2 \sin\theta\, \mathrm{d}\theta\right\}^{1/2} \tag{113}$$

where ϕ^h is the approximate finite element solution and ϕ is the exact steady state solution. Figure 5 gives the relative maximum L_2 error

$$E_{\max} = \max_{t_1 \leqslant t \leqslant t_2} E(t) \tag{114}$$

over the steady-state interval $t \in (t_1, t_2) = (10, 30)$, computed using RBC1$(6,P)$, $P = 1, 2, \ldots, 6$, normalized with the exact condition RBC1$(6,6)$.

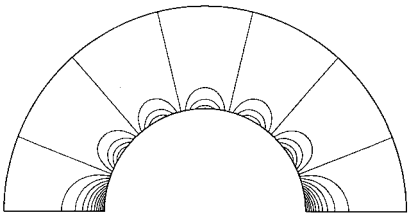

Figure 3. Spherical harmonic $n=6$ with normalized frequency $\omega a/c=\pi/4$. Solution contours at $t=42.64$, using RBC1(6,6).

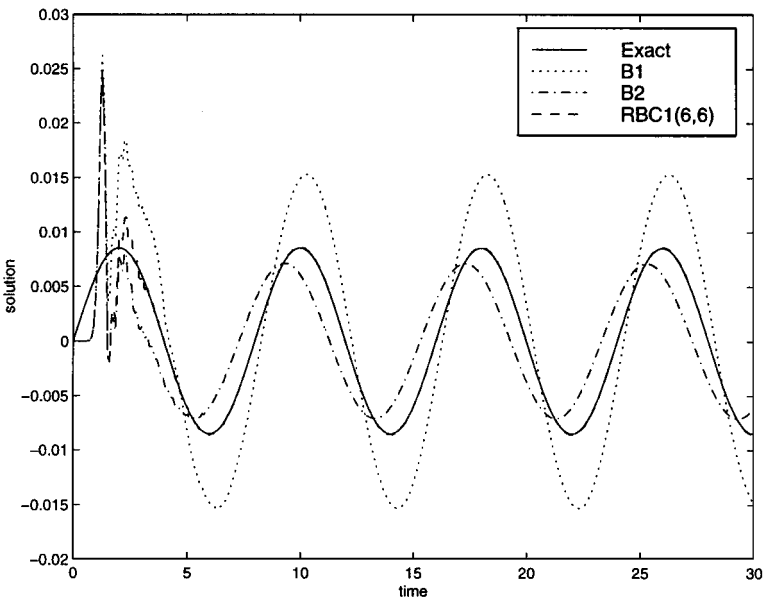

Figure 4. Spherical wave harmonic $n=6$; frequency $\omega a/c=\pi/4$. Time-dependent solutions computed using the local radiation boundary conditions B_1, B_2, and RBC1(N,P), with truncated expansion $N=6$, and $P=N$. Numerical results are compared to the steady state exact solution on Γ at $R/a=2$, and $\theta=0^\circ$.

Solutions are compared at three different frequencies, $\omega a/c=[\pi/4,\pi,2\pi]$, with corresponding time-steps $\Delta t=[0.08,0.02,0.01]$. These results demonstrate that for the low frequency value, the accuracy using the uniform approximation RBC1$(6,P)$, with $P=5$, is almost the same as the exact condition RBC1$(6,6)$. As the frequency is increased, the number of auxiliary variables needed to approach the exact condition is reduced significantly. In particular, for $\omega a/c=2\pi$, then the asymptotic radiation boundary condition RBC1$(6,2)$ with value $P=2$, is sufficient to accurately represent the exact condition corresponding to $P=6$. For this test problem, the accuracy of RBC1$(6,2)$ is equivalent to using a local third-order B_3 Bayliss and Turkel boundary condition.

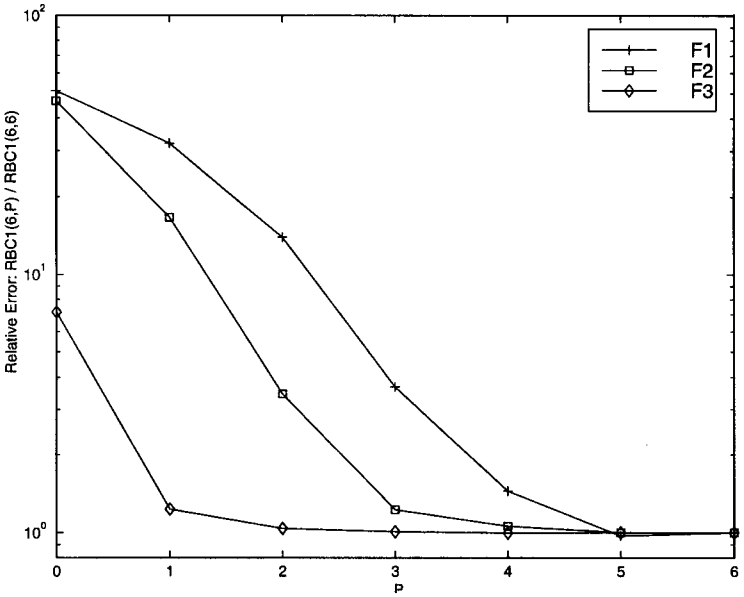

Figure 5. Harmonic $n=6$. Relative maximum L_2 error RBC1$(6,P)$/RBC1$(6,6)$, on the radiation boundary Γ during steady state. Comparisons for frequences $\omega a/c=[F1,F2,F3]=[\pi/4,\ \pi,\ 2\pi]$.

5.2. *Transient radiation from a piston on a sphere*

To study the accuracy for a problem involving an infinite number of spherical harmonics, we consider axisymmetric radiation from a circular piston on a sphere with radius $a=0.5$. The piston is represented by the Dirichlet condition

$$\phi(a,\theta,t)=f(\theta)\ \sin\omega t\, H(t), \quad 0\leqslant\theta\leqslant\pi \tag{115}$$

where $H(t)$ is the Heaviside function and

$$f(\theta)=\begin{cases} 1, & 0^\circ\leqslant\theta\leqslant\theta_1 \\ \dfrac{\cos\ \theta-\cos\ \theta_2}{\cos\theta_1-\cos\theta_2}, & \theta_1\ <\ \theta\leqslant\theta_2 \\ 0 & \text{otherwise} \end{cases} \tag{116}$$

For this example, we set $\theta_1=15^\circ$, and $\theta_2=30^\circ$. This problem is challenging because the waves radiated at the piston pole $\theta=0^\circ$ are attenuated by a geometric spreading loss as they travel along longitudes down to the south pole $\theta=180^\circ$. In the region opposite the piston (shadow zone), the amplitude of the waves are significantly lower than near the piston [33]. The exact transient solution to this problem contains a term decreasing rapidly with time which can be explained due to the presence of 'creeping waves', i.e. the radiation from the piston can encircle the sphere a number of times, so that the transient solution in principle never reaches a steady state, although in practice the exponentially decreasing term quickly becomes negligible as time increases.

The exact steady state solution to this problem is obtained by expanding the function $f(\theta)$ as a series of Legendre functions P_n, and evaluating the radiated solution at $r=a$, with the

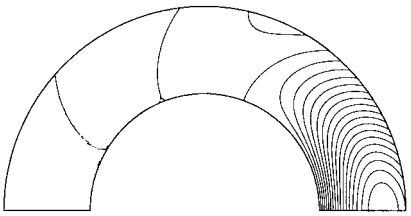

Figure 6. Radiation from a piston on a sphere with radius $a = 0.5$ and frequency $\omega a/c = \pi$. Solution contours at steady state, using RBC1(20, 20). Radiation boundary Γ set at $R/a = 1.75$.

result

$$\phi(r, \theta, t) = -\,\mathrm{Imag}\left\{ \mathrm{e}^{-\mathrm{i}\omega t} \sum_{n=0}^{\infty} A_n \frac{h_n(kr)}{h_n(ka)} P_n(u) \right\} \tag{117}$$

with coefficients

$$A_0 = \tfrac{1}{4}(2 - u_1 - u_2) \tag{118}$$

and for $n \geqslant 1$

$$A_n = \frac{1}{2}[P_{n-1}(u_1) - P_{n+1}(u_1)] + \frac{2n+1}{2} \int_{u_1}^{u_2} \frac{u_2 - u}{u_1 - u_2} P_n(u)\, \mathrm{d}u \tag{119}$$

where $u = \cos\theta$. In the above, the integral is evaluated exactly using $n/2 + 1$ Gauss–Legendre quadrature points.

For this problem, the spherical radiation boundary Γ, is positioned at three different locations defined by $R/a = [1.25, 1.5, 1.75]$, with corresponding meshes of $[10, 20, 30] \times 240$ elements evenly spaced in the region $(0.5 \leqslant r \leqslant R), \times (0 \leqslant \theta \leqslant \pi)$. The computation is driven from rest to steady state with a normalized frequency $\omega a/c = \pi$ and a time step $\Delta t = 0.005$.

For reference, Figure 6 shows contours of the numerical solution using RBC1(20, 20) positioned at $R/a = 1.75$, for a representative time $t = 4$, during steady state. Figure 7 shows the solution at the observation point $R/a = 1.75$ and $\theta = 180°$, located in the shadow zone on the backside of the piston. In this difficult region, the solution using B_1 and B_2 exhibits large spurious reflections, while the solution using RBC1(20, 20) gives accurate solutions.

Figure 8 (Top) shows the maximum L_2 error for RBC1(N, N) measured on a sphere with radius $R_0/a = 1.25$, when the radiation boundary condition is moved from $R/a = 1.25$ to $R/a = 1.75$, and the number of modes included in the radiation boundary condition N, increasing from 0 to 20. We observe that the solutions using RBC1(N, N) converge to approximately the same minimum error value for each truncation boundary position. This limiting error is controlled primarily by the discretization of the spherical harmonic transforms. With the number of grid points on the boundary, $N_\Gamma = 240$, and $N = 20$, we have $N_\Gamma/N = 12$ grid points/mode. As the truncation boundary is moved further away from the source, the number of modes N required to obtain a fixed level of accuracy is reduced. For example, for $R/a = 1.25$, $N = 20$ terms are needed to converge, whereas, when R/a is increased to 1.75, only $N = 9$ terms are required. Figure 8 (Bottom) shows the maximum error using RBC1(N, P) for fixed $N = 20$, and with variable $P \leqslant 20$. These results show that accurate solutions are obtained using a value of P significantly lower than N, with corresponding reduction in work and memory.

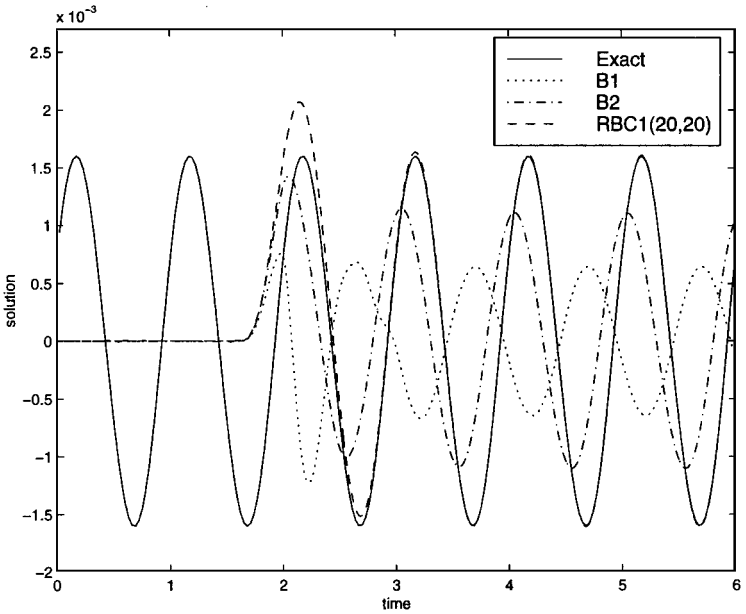

Figure 7. Time-histories at observation point on $R/a = 1.75$, and $\theta = \pi$.

For the axisymmetric case, with $m = 0$, the total number of auxiliary equations for RBC1(N,P) is $O(PN)$:

$$N_p = \sum_{n=1}^{P} n + (N-P)P = \frac{1}{2}P(2N - P + 1) \tag{120}$$

and for the exact condition RBC1(N,N), the number increases to $O(N^2)$:

$$N_p = \sum_{n=1}^{N} n = \frac{1}{2}N(N+1) \tag{121}$$

In particular, for the case where the truncation boundary Γ is positioned close to the source $(R/a = 1.25)$, such that $N = 20$ modes are needed to obtain accurate solutions, then $P = 5$ is sufficient to converge to the same limiting error value, i.e. the error in RBC1$(20,20) \approx$ RBC1$(20,5)$. The total number of auxiliary equations using the exact condition RBC1$(20,20)$ is $\sum_{n=1}^{20} n = 210$, while RBC1$(20,5)$ only requires $\sum_{n=1}^{5} n + 5(20-5) = 90$ equations, a significant reduction. In general, we observe that $P \geqslant N/3$ is sufficient to approximate the accuracy of the exact condition.

5.3. Transient scattering of a plane wave by a sphere

To study the total field solution to the scattering problem, consider a sphere of radius $a = 1$, on which we assume a homogeneous Neumann boundary condition

$$\frac{\partial \phi}{\partial r} = 0, \quad \text{on } r = a \tag{122}$$

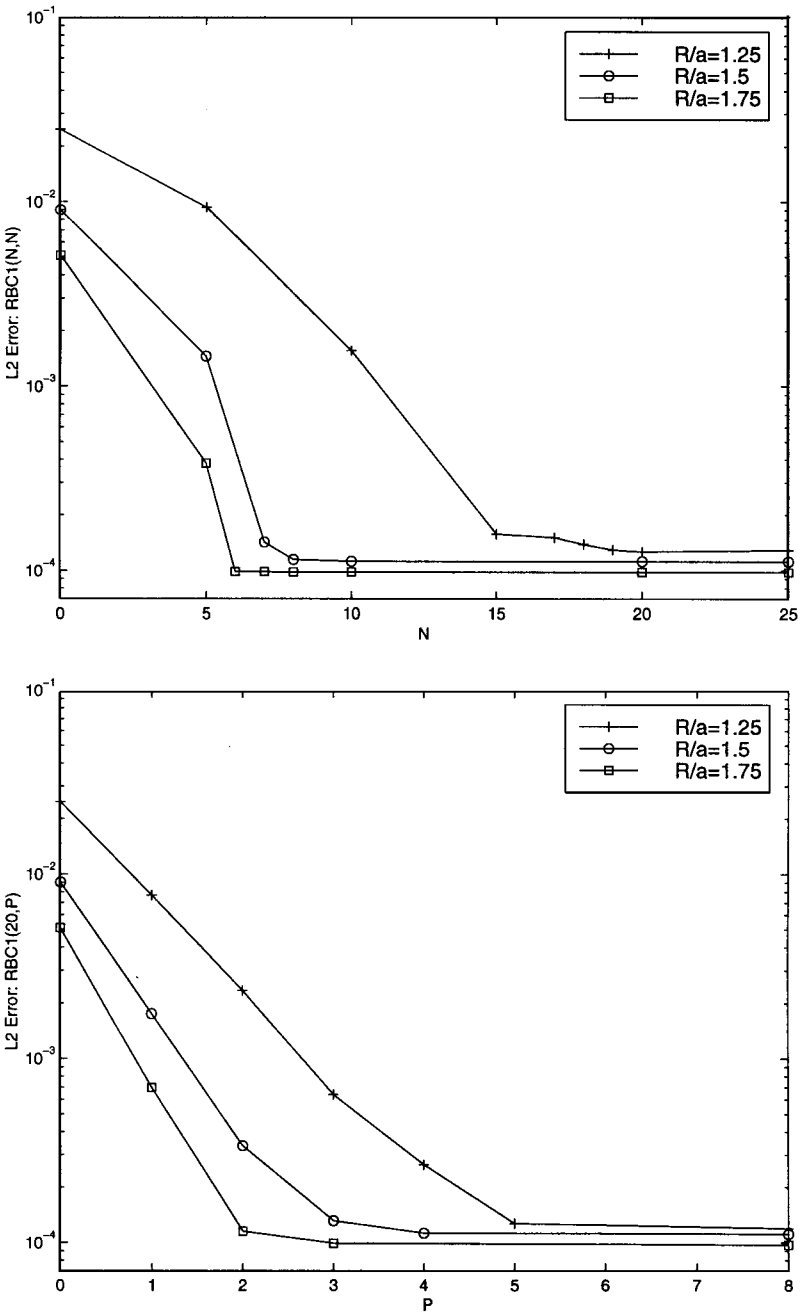

Figure 8. Radiation from piston on a sphere of radius $a = 0.5$ and frequency $\omega a/c = \pi$. Maximum L_2 error during steady state measured at $r/a = 1.25$. Radiation boundary condition applied at truncation boundary Γ postioned at $R/a = 1.25, 1.5, 1.75$. Numerical solutions using (top): RBC1(N, N), (bottom): RBC1$(20, P)$.

If ϕ is the acoustic pressure, this condition represents a 'rigid' scatterer. Let the incident wave be represented by a traveling plane wave along the z-axis at speed c, i.e.

$$\phi^{(i)} = \begin{cases} \sin[k(z - z_0) - \omega t], & t \geqslant \dfrac{z - z_0}{c} \\ 0, & t < \dfrac{z - z_0}{c} \end{cases} \tag{123}$$

Here $k = \omega/c$, and the wave is incident from the $\theta = \pi$ direction, and z_0 is the location of the plane wave at time $t = 0$. The total field $\phi(r, \theta, t)$ is composed of a superposition of the incident wave $\phi^{(\mathrm{i})}(z, t)$ and a scattered wave $\phi^{(\mathrm{s})}(r, \theta, t)$, i.e. $\phi = \phi^{(\mathrm{i})} + \phi^{(\mathrm{s})}$. With the Neumann boundary condition (122), the scattered field is a solution to the wave equation subject to the boundary condition

$$\frac{\partial \phi^{(\mathrm{s})}}{\partial r} = -\frac{\partial \phi^{(\mathrm{i})}}{\partial r} = -k \cos u \cos \theta H\left(t - \frac{z - z_0}{c}\right) \quad \text{on } r = a \tag{124}$$

and $u = k(z - z_0) - \omega t$, $z = a \cos \theta$.

The exact steady state solution is obtained by expanding the exponential form of the incident wave in spherical harmonics by means of an addition theorem [33]. For $\phi^{(i)}$ given in (123), the steady state analytical solution is

$$\phi^{(\mathrm{s})}(r, \theta) = \mathrm{Imag}\left\{ \mathrm{e}^{-\mathrm{i}(kz_0 + \omega t)} \sum_{n=0}^{\infty} A_n h_n(kr) P_n(\cos \theta) \right\} \tag{125}$$

$$A_n = -\mathrm{i}^n (2n + 1) \frac{j_n'(ka)}{h_n'(ka)} \tag{126}$$

In the above, j_n and h_n are spherical Bessel's and Hankel's functions of the first kind respectively.

For the finite element solution, we use the modified variational equation for the total field where the incident wave is represented on the radiation boundary Γ. For the incident wave defined in (123), the modification to the boundary operator $\mathbf{F}_\Gamma$ given in Equation (88) involves the inner product with

$$B_1 \phi^{(\mathrm{i})} = \left[k \cos u (\cos \theta - 1) + \frac{1}{R} \sin u \right] H\left(t - \frac{z - z_0}{c}\right), \tag{127}$$

and $z = R \cos \theta$. The bounded domain is discretized with a uniform mesh of standard four-node bilinear axisymmetric finite elements with 240 evenly spaced elements in $0 \leqslant \theta \leqslant \pi$. The radiation boundary is placed at three different radii $R/a = [1.25, 1.5, 1.75]$, with corresponding mesh $240 \times [10, 20, 30]$. The computation is driven from rest at $z_0 = -2$, to steady state with a normalized frequency $\omega a/c = \pi$ and a time step $\Delta t = 0.01$.

Contours for the scattered solution $\phi^{(\mathrm{s})} = \phi - \phi^{(\mathrm{i})}$, computed using RBC1(10, 10) positioned at $R/a = 1.75$ are shown in Figure 9. Figure 10 shows time histories of the scattered solution on the artificial boundary Γ defined by $R/a = 1.25$, both at $\theta = 0$, and the backscattered point $\theta = \pi$. Results are compared using the local operators B_1, B_2 and RBC1(10, 10). At the backscattered point, the solutions using B_2 and RBC1(10, 10) can barely be distinguished with the exact steady state solution. Results for B_1 show small errors in amplitude and phase. However, on the other side of the sphere, at point $\theta = 0$, both operators B_1 and B_2 exhibit significant spurious reflection. In contrast, the solution using RBC1(10, 10) matched the exact solution very well.

Figure 11 shows the maximum L_2 error during steady state measured on a sphere with radius $R_0/a = 1.25$. For this example, we observe that the solutions using RBC1(N, N) converge rapidly

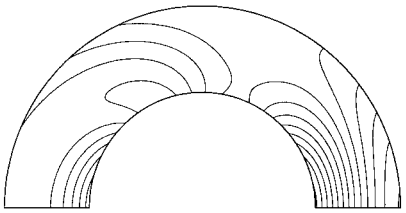

Figure 9. Scattering from a sphere with wave incident from the ($\theta = \pi$) direction, and normalized frequency $\omega a/c = \pi$. Solution contours at steady state ($t = 15$), using RBC1(10, 10) and $R/a = 1.75$.

with N. As the radiation boundary is moved further away from the source, the number of modes N required to obtain a fixed level of accuracy is reduced. For $R/a = 1.25$, $N = 8$ modes are needed to converge. As the radiation boundary is moved further away from the scatterer to $R/a = 1.75$, then only $N = 6$ modes are needed. The maximum error using RBC1(N, P) for fixed $N = 8$, and with variable $P \leqslant 6$, is shown in Figure 11 (Bottom). These results again show that the uniform approximation to the exact condition is sufficiently accurate with $N/3 \leqslant P \leqslant N$.

5.4. *Transient radiation from a circular piston in infinite planar baffle*

In this example we study transient radiation in a semi-infinite region defined by circular transducer of radius $a = 1$ mounted in an infinite rigid planar baffle. A circular transducer radiating into an acoustic fluid is considered since this case has been widely studied and is important to many researchers. Let ϕ denote acoustic pressure, then the sound pressure field is determined by the wave equation and by the boundary conditions

$$\frac{\partial \phi}{\partial z} = \begin{cases} -\rho_0 \dot{v}(t) & \text{on piston } \mathsf{P} = \{0 \leqslant r \leqslant a, \theta = \pi/2\} \\ 0 & \text{on baffle } \mathsf{B} = \{r > a, \theta = \pi/2\} \end{cases} \tag{128}$$

where z is the coordinate normal to the piston and baffle, $v(t)$ is the velocity of the piston, and a superimposed dot denotes a time derivative. The normal velocity is assumed to be the Gaussian pulse

$$v(t) = \mathrm{e}^{-0.5 f_0^2 (t - t_0)^2} H(t) \tag{129}$$

where $t_0 = 0.5$ s, and $f_0 = 8$ and wave speed $c = 1$. With this choice of parameters, the wavelet spans the time interval of $t \in (0, 1)$ s and excites a continuous band of frequencies over the range $\omega \in (0, 25)$ rad/s.

The solution $\phi(r, \theta, t)$ is rotationally symmetric about the z-axis normal to the center of the piston. Since the problem is axisymmetric, it is convenient to introduce cylindrical co-ordinates (ρ, z), where $\rho = \sqrt{x^2 + y^2}$ is the polar radius (distance off the axis) of the circular piston. The analytic solution to this problem is obtained by means of an impulse response function $h(\rho, z, t)$ which is derived by Stepanishen [34] for a circular piston:

$$\phi(\rho, z, t) = -\rho_0 \frac{\partial}{\partial t} [v(t) * h(\rho, z, t)] \tag{130}$$

where ρ_0 is the density of the medium, and the asterisk is used to denote convolution in time. For observation points on the z-axis, the time convolution may be evaluated in closed form. Points off-axis are integrated numerically. For this input, the solution on the z-axis consists of two Gaussian

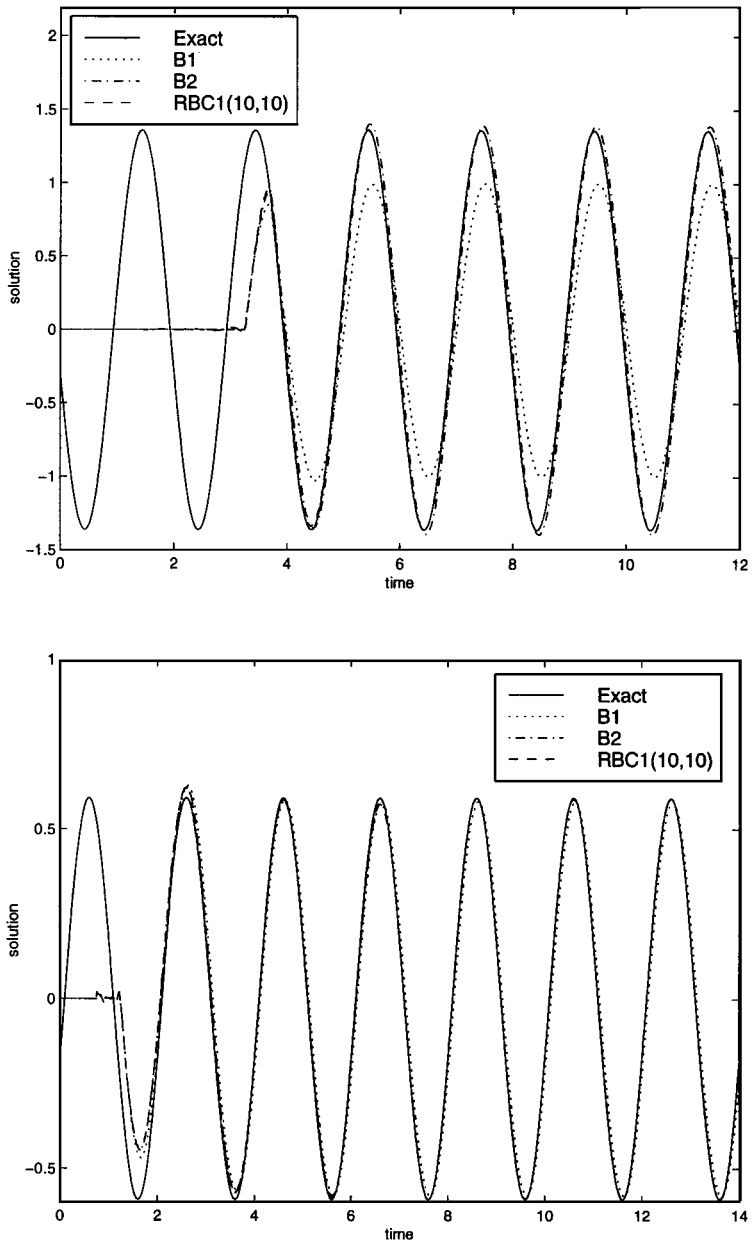

Figure 10. Scattering of plane wave from a sphere. Time histories on the artificial boundary Γ, at (top) $\theta = 0$, and (bottom) backscattered point $\theta = \pi$. Results compared for local operators B_1, B_2 and RBC1(N,P) with $N = P = 10$.

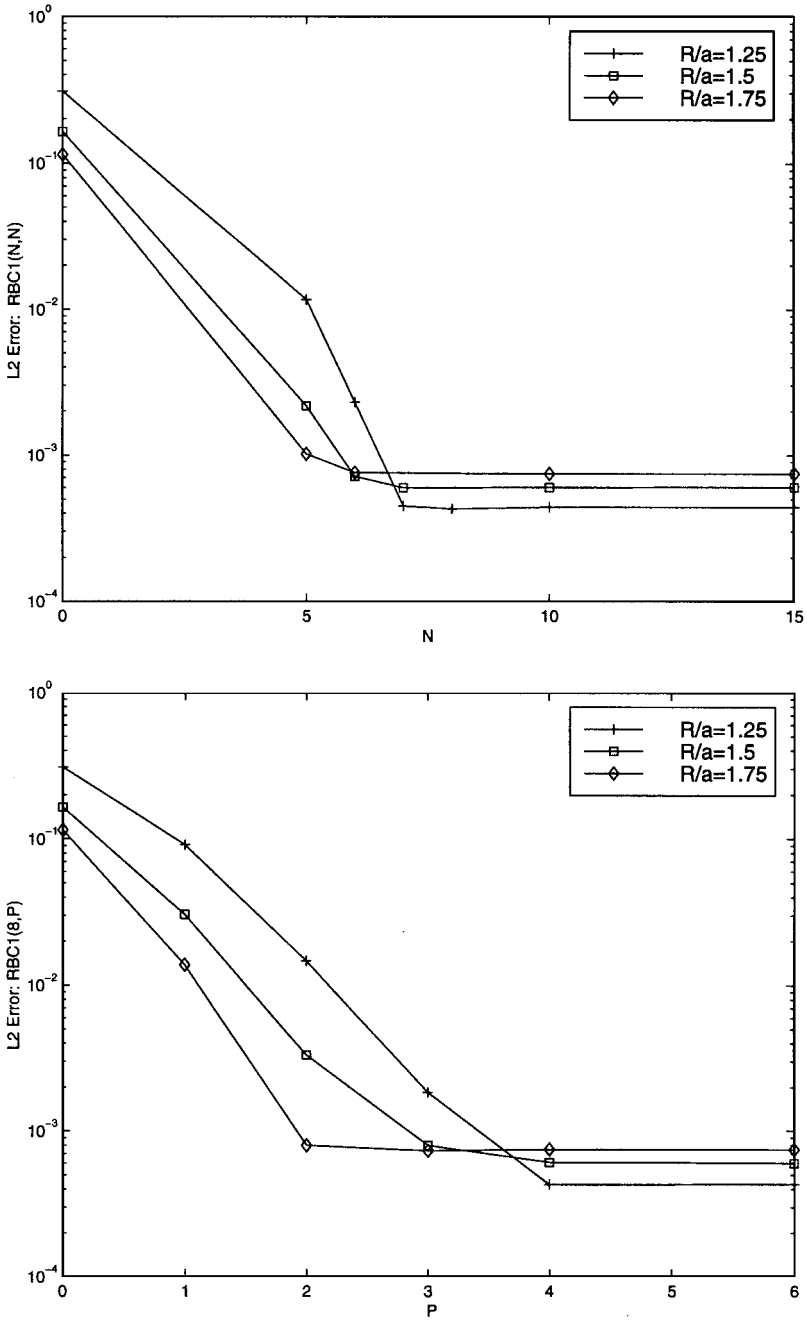

Figure 11. Scattering of a plane-wave from a sphere. Maximum L_2 error during steady state measured at $r/a = 1.25$. Radiation boundary condition applied at truncation boundary Γ postioned at $R/a = 1.25, 1.5, 1.75$. Numerical solutions using (top): RBC1(N, N), (bottom): RBC1$(8, P)$.

pulses of opposite amplitude. The time delay of the initial pulse corresponds to the propagation time from the centre of the piston to the spatial point, and the time delay of the second pulse corresponds to the propagation time from the edge of the piston to the spatial point.

To satisfy the symmetry condition at the rigid baffle, it is sufficient to restrict the indices appearing in the expansion for the RBC1 defined in (111) to $n=$ even, and modify the transform (112) for the radial harmonics by a factor of two, with integration restricted over the interval $0 \leqslant \theta < \pi/2$. To provide a challenging problem, the truncation boundary Γ is positioned near the edge of the circular piston with $R/a = 1.25$. The finite element mesh consists of 150 evenly spaced axisymmetric elements along the z-axis from $0 \leqslant z \leqslant 1.25$, and 90 evenly spaced elements from $0 < \theta \leqslant \pi/2$. The time step is set at $\Delta t = 0.015$.

Figure 12 shows contours of the pressure field solution using RBC1(20, 20) at several time steps. The solution obtained using RBC1(20, 20) is nearly identical to the analytical solution at all observation points. Figure 13 shows transient solutions at several observation points on the z-axis and different locations on the truncation boundary Γ. Comparisons are made between the analytical solution and numerical solutions using the asymptotic radiation boundary condition RBC1$(20, P)$ with $P = 0, 1$ and $P = 3$. For this example problem, with $N = 20$ angular harmonics included in the expansion, the accuracy of condition RBC1(20, 0) is nearly identical to the local B_1 operator of Bayliss and Turkel. Similarly, RBC1(20, 1) behaves like the local B_2 operator. The accuracy of condition RBC1(20, 3) is expected to be approximately the same as the local B_4 operator. The results indicate that the early time response is accurately represented on the z-axis using any of the boundary conditions studied. However, the numerical solution for RBC1(20, 0) and RBC1(20, 1) exhibits large errors at later times; both overshooting and undershooting the exact solution. At angles off the piston axis, the conditions RBC1(20, 0) and RBC1(20, 1) exhibit spurious reflections during both the initial and secondary pulses. The RBC1(20, 3) condition matches the analytical solution well for both early and late times, both on- and off-axis. This result shows that with the mesh used, the angular harmonics are resolved accurately, and accurate solutions are obtained with the asymptotic form of RBC1(N, P). In this case it is sufficient to use a small number ($P = 3$) of auxiliary functions.

6. CONCLUSIONS

Asymptotic and exact local radiation boundary conditions first derived by Hagstrom and Hariharan for the time-dependent wave equation, are rederived based on the hierarchy of local boundary operators used by Bayliss and Turkel and a recursion relation for the expansion coefficients appearing in the asymptotic (multipole) expansion for radial wave harmonics. By introducing a decomposition into spherical harmonics we reformulate the sequence of local boundary conditions as a Cauchy problem involving systems of first-order temporal equations, similar to that used in References [10, 12]. A modified version similar to the formulation given in Reference [13] is also reported. With this reformulation, the auxiliary functions are recognized as residuals of the local boundary operators acting on the asymptotic expansion. The use of spherical harmonics allows the boundary conditions to be implemented efficiently and concurrently without altering the local character of the finite element equations. With the number of time-dependent auxiliary variables in the Cauchy problem for each harmonic equal to the mode number, the RBCs are exact. If fewer equations are used, then the boundary conditions form high-order accurate asymptotic approximations to the exact condition, with corresponding reduction in work and memory. Computation of eigenvalues

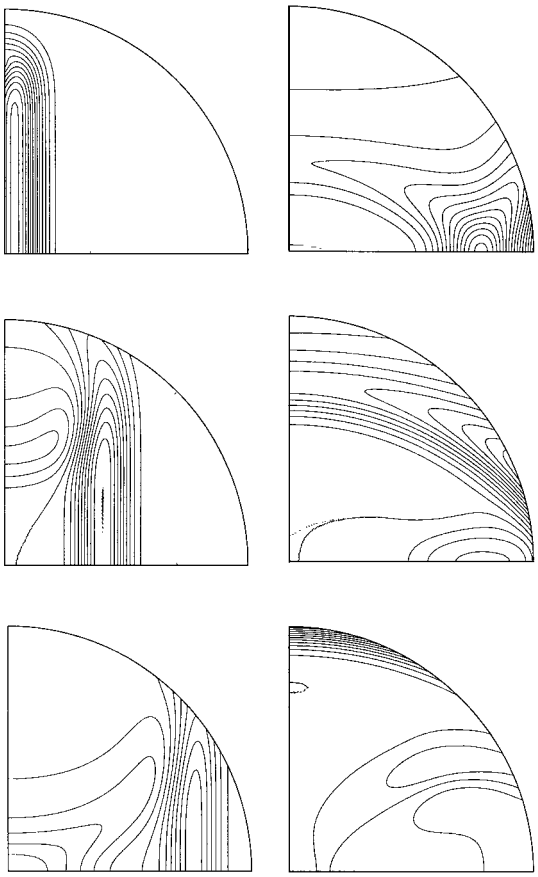

Figure 12. Solution contours of pressure field using RBC1(20, 20) for transient radiation from a circular piston in infinite planar baffle at time (left): (a) $t = 0.45$; (b) $t = 0.9$; (c) $t = 1.35$. (right): (a) $t = 1.8$; (b) $t = 2.25$; and (c) $t = 2.7$.

for the first-order system of residual functions verified solutions are stable. Using a linear transformation, we establish the equivalence of our exact version of the RBC to the non-reflecting boundary conditions (NRBC) derived in References [10, 12]. Our analysis of the NRBC provides a straightforward derivation and a clear physical interpretation of the auxiliary functions, here interpreted as wave functions appearing in the multipole expansion. Several improvements of our radiation boundary condition over the NRBC derived in References [10, 12] have been identified including a banded tri-diagonal coefficient matrix for the auxiliary variables, reduced memory and computational work needed to store and solve the auxiliary functions for each harmonic, and the ability to vary separately the radial and transverse modal orders of the radiation boundary condition. Furthermore, using asymptotic radial wave expansions and Fourier modes similar to that used in this paper for the three-dimensional wave equation, we have developed an efficient finite element implementation on a circle in two dimensions [35].

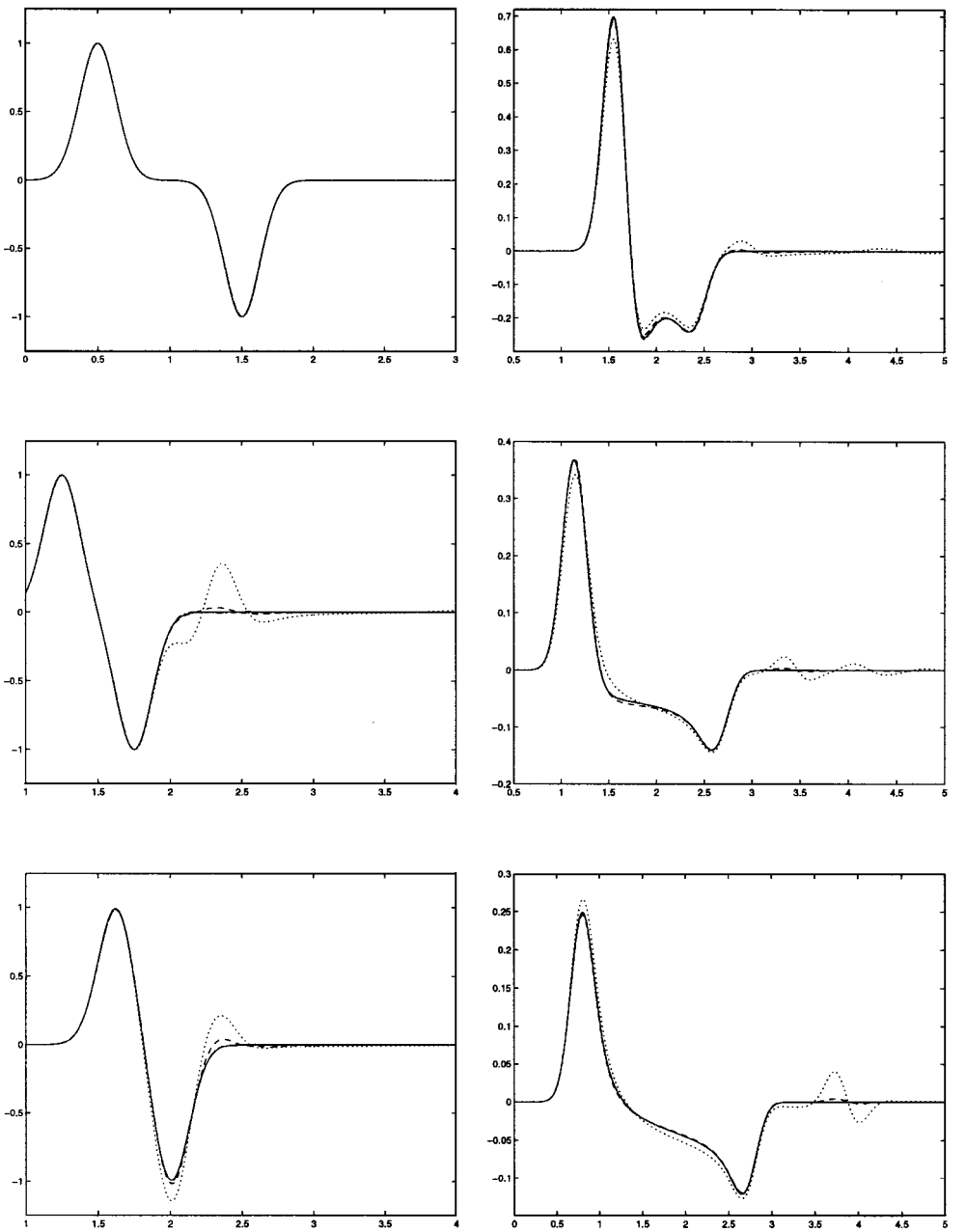

Figure 13. Time histories at observation points: (left) On-axis at $\theta = 0$, $z = 0.0, 0.75, 1.125$; (right) Off-axis on Γ at $R = 1.25$, $\theta = 30, 60, 90^\circ$. Solid line denotes analytic solution; Dotted line denotes RBC1$(20, 0)$; Dashed line denotes RBC$(20, 1)$; Dashed-dotted line denotes RBC1$(20, 3)$.

For scattering problems, a finite element formulation for the total field, which avoids explicitly computing normal derivatives on a geometrically complex scattered surface is presented. With this formulation, the variational equation is modified by including the incident wave field on the spherical radiation boundary. On a sphere, the normal derivative simplifies to a radial derivative which can easily be computed a priori. Furthermore, we show how the spherical harmonics appearing in the RBC may be approximated with a projection onto a finite-dimensional basis using the same shape functions used for the finite element mesh. In this form, arrays appearing in the inner products of the boundary operator may be diagonalized for efficiency. The RBC's may be computed using standard nodal or element assembly procedures with mixed time integration algorithms similar to that used in References [12–14]. The maximum number of spherical harmonics needed to obtain accurate results is usually smaller than the number of grid points on the radiation boundary. As a result, the work and amount of memory needed to store the auxiliary functions is negligible when compared to the storage required for the solution in the interior domain. If a large number of harmonics are needed, the work required can be reduced by an order of magnitude by using recently developed fast spherical harmonic transform methods.

Since the RBC is based on an asymptotic expansion of radial modes, the accuracy rapidly converges with the number of residual functions included in the Cauchy problem. Numerical studies both for individual harmonics, and radiation/scattering problems involving an infinite number of modes demonstrate that the asymptotic form of the radiation boundary condition show dramatically improved accuracy for time domain simulations compared to the first- and second-order local boundary operators of Bayliss and Turkel and improved efficiency over the exact condition. Further research is needed to obtain strong a priori estimates in integral norms for the accuracy of the asymptotic version of the boundary conditions, as a function of the number of residual functions included.

ACKNOWLEDGEMENTS

Support for this work was provided by the National Science Foundation under Grant CMS-9702082 in conjunction with a Presidential Early Career Award for Scientists and Engineers (PECASE), and is gratefully acknowledged.

REFERENCES

1. Mitzner KM. Numerical solution for transient scattering from a hard surface of arbitrary shape—Retarded potential technique. *Journal of the Acoustical Society of America* 1967; **42**:391–397.
2. Farn CLS, Huan H. Transient acoustic fields generated by a body of arbitrary shape. *Journal of the Acoustical Society of America* 1968; **43**:252–257.
3. Groenenboom PHL. Solution of the retarded potential equation and numerical stability. In *Boundary Elements VI, Proceedings of 6th International Conference*, Brebbia CA (ed.). July 1984.
4. Dyka CT, Ingel RP, Kirby GC. Stabilizing the retarded potential method for transient fluid-structure interaction problems. *International Journal for Numerical Methods in Engineering* 1997; **40**:3767–3783.
5. Givoli D. Non-reflecting boundary conditions, a review. *Journal of Computational Physics* 1991; **94**:1–29.
6. Tsynkov S. Numerical solution of problems on unbounded domains. A review. *Applied Numerical Mathematics* 1998; **27**:465–532.
7. Bayliss A, Turkel E. Radiation boundary conditions for wave-like equations. *Communications in Pure and Applied Mathematics* 1980; **33**:707–725.
8. Ting L, Miksis M. Exact boundary conditions for scattering problems. *Journal of the Acoustical Society of America* 1986; **80**:1825–1827.
9. Givoli D, Kohen D. Non-reflecting boundary conditions based on Kirchoff-type formulae. *Journal of Computational Physics* 1995; **117**:102–113.

10. Grote MJ, Keller JB. Exact non-reflecting boundary conditions for the time dependent wave equation. *SIAM Journal of Applied Mathematics* 1995; **55**:280–297.
11. Grote MJ, Keller JB. Nonreflecting boundary conditions for time dependent scattering. *Journal of Computational Physics* 1996; **127**:52–65.
12. Thompson LL, Huan R. Implementation of exact non-reflecting boundary conditions in the finite element method for the time-dependent wave equation. *Computer Methods in Applied Mechanics and Engineering*, in press.
13. Thompson LL, Huan R. Finite element formulation of exact non-reflecting boundary conditions for the time-dependent wave equation. *International Journal for Numerical Methods in Engineering* 1999; **45**:1607–1630.
14. Thompson LL, Huan R. Computation of transient radiation in semi-infinite regions based on exact nonreflecting boundary conditions and mixed time integration. *Journal of the Acoustical Society of America* 1999; **106**(6):3095–3108.
15. Thompson LL, Huan R. Computation of far field solutions based on exact nonreflecting boundary conditions for the time-dependent wave equation. *Computer Methods in Applied Mechanics and Engineering*, in press.
16. Alpert B, Greengard L, Hagstrom T. Rapid evaluation of nonreflecting boundary kernels for time-domain wave propagation. *SIAM Journal on Numerical Analysis*, to appear.
17. Berenger JP. A perfectly matched layer for the absorption of electromagnetic waves. *Journal of Computational Physics* 1994; **114**:185–200.
18. Xiaojuen Yuan, Borup D, Wiskin JW, Berggren M, Eidens R, Johnson SA. *Formulation and Validation of Berenger's PML Absorbing Boundary for the FDTD Simulation of Acoustic Scattering*, IEEE Transactions on Ultrasonics, Ferro, Frequencey Control, vol. 44, No. 4, July 1997; 517–522.
19. Hagstrom T, Hariharan S. A formulation of asymptotic and exact boundary conditions using local operators. *Applied Numerical Mathematics* 1998; **27**:403–416.
20. Keller JB, Givoli D. Exact non-reflecting boundary conditions. *Journal of Computational Physics* 1989; **82**:172–192.
21. Pearson LW, Whitaker RA, Bahrmasel LJ. An exact radiation boundary condition for the finite-element solution of electromagnetic scattering on an open domain. *IEEE Transactions on Magnetics* 1989; **25**(4):3046–3048.
22. Thompson LL. Finite element methods for time-harmonic structural acoustics in exterior domains: derivation of exact DtN maps for elliptic and spheroidal radiation boundaries. *ONR Contract Review Meeting*, Stanford University, Stanford, CA, 19 April 1994. *Technical Report: CMCU-94-01*, Advanced Computational Mechanics Laboratory, Clemson University, August 1994.
23. Grote MJ, Keller JB. On nonreflecting boundary conditions. *Journal of Computational Physics* 1995; **122**:231–243.
24. Ben-Porat G, Givoli D. Solution of unbounded domain problems using elliptic artificial boundaries. *Communications in Numerical Methods in Engineering* 1995; **11**:735–741.
25. Thompson LL, Huan R, Ianculescu C. Finite element formulation of exact Dirichlet-to-Neumann radiation conditions on elliptic and spheroidal boundaries. *Proceedings of the ASME Noise and Acoustics Division - 1999*, The American Society of Mechanical Engineers, **NCA-Vol. 26**, 497–509.
26. Sofronov I. Artificial boundary conditions for absolute transparency for two- and three-dimensional external time-dependent scattering problems. *European Journal of Applied Mathematics* 1998; **9**(6):561–588.
27. Thompson LL, Pinsky PM. New space-time finite element methods for fluid-structure interaction in exterior domains. *Computational Methods for Fluid/Structure Interaction*, ASME 1993; **AMD-178**:101–120.
28. Thompson LL, Pinsky PM. A space-time finite element method for structural acoustics in infinite domains, Part 2: Exact time-dependent non-reflecting boundary conditions. *Computer Methods Applied in Mechanics and Engineering* 1996; **132**:229–258.
29. Lamb H. *Hydrodynamics* (4th edn). Cambridge University Press: Cambridge, 1916; 517, eq. 4.
30. Brown TM. Solar rotation as a function of depth and latitude. *Nature* 1985; **317**(17):591–594.
31. Mohlenkamp MJ. A fast transform for spherical harmonics. *The Journal of Fourier Analysis and Applications* 1999; **5**(2-3):159–184.
32. Driscoll J, Healy D, Rockmore D. Fast discrete polynomial transforms with applications to data analysis for distance transitive graphs. *SIAM Journal of Computing* 1997; **26**:1066–1099.
33. Morse PM, Feshbach H. *Methods of Theoretical Physics*, vol II. McGraw-Hill: New York, 1953.
34. Stepanishen PR. Transient radiation from pistons in an infinite planar baffle. *Journal of the Acoustical Society of America* 1977; **49**:1629–1638.
35. Thompson LL, Huan R. Accurate radiation boundary conditions for the two-dimensional wave equation on unbounded domains. 1999; submitted.

